School of Chemistry, Chemical Engineering and Biotechnology

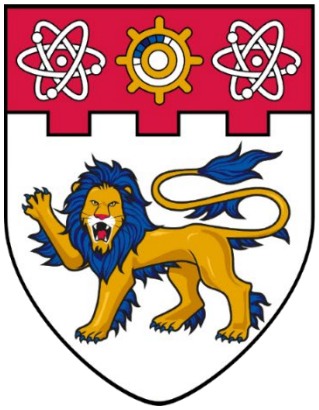

NANYANG TECHNOLOGICAL UNIVERSITY
SINGAPORE

CH 4801

FYDP Report

Group 1.1

Name	Matric No.
Lim Junwei Darien	U1921811F
Cassandre Chan Xiao Ying	U1921686H
Teo Jun Wei	U1921624E
Indhu Jayabaskaran	U1922186D
Ang Cheng Ting	U1922234G
Ashley Soh Wem Qi	U1922862A
Er Wei Leong Leonard	U1920209F
Yap Yan Lin	U1922551K

Content Page

Executive Summary

In this report, we designed a greener recycling process for the recycling of Nickel Manganese Cobalt (NMC) based Lithium-Ion Batteries (LIBs). The process will occur in batches, and the plant will operate 330 days a year, 4 batches a day. 5411.26 kg of batteries will be processed per batch. Black mass that enters the plant will first undergo a series of pre-treatment processes to separate the different cell materials. After separation of the cell products, products such as graphite and copper were sold, while the active cathode materials require further processing. The active cathode materials will then undergo leaching by oxalic acid (OA). The precipitate will subsequently undergo a second leaching by sulfuric acid (SA). Further precipitation was done with the addition of Potassium Carbonate and Magnesium Oxide, where Lithium Carbonate (97.8% purity) and mixed hydroxides (88.2% purity) are produced which can be sold. The Dominant Design Variables (DDVs) of the process were identified and ranked. The main DDV, SA pulp density, was varied and optimised with other Design Variables (DVs) to obtain the optimised process case. A Hazard and Operability study (HAZOP) was carried out to ensure safe operations, and proper waste management was done to prevent negative impacts on human health and the environment. Although the aim of this project was to design an economical and green process to recycle 5000 metric tonnes per annum of spent Li-ion batteries, economic analysis was also performed, and the findings indicates that the plant is not feasible to construct.

1. Motivation, Market Analysis and Objectives

1.1. Motivation

Currently, existing vehicles use an internal combustion engine (ICE) powered by fuel combustion, releasing gases like sulfur oxide and hydrocarbons — significant contributors to air pollution and global warming. Hence, the 27th Conference of the Parties to the United Nations Framework Convention on Climate Change (COP27) proposed to accelerate the transition to zero emission vehicles by 2035 in leading markets, and 2040 globally [1, 2]. Electric vehicles (EVs) are on the rise as electrification is believed to be a key technological strategy to reduce air pollution and greenhouse gas emission. LIBs enable the new generation of EVs to be commercialized by global automakers. LIBs are a type of rechargeable battery which use reversible reduction of lithium ions to store energy, preferred for their large energy storage capacity and high-power performance [3].

1.2. Market Analysis and Project Objective

The growing market for LIBs raises the concern of sustainable management of spent battery waste and key metals such as lithium, copper, nickel and cobalt. The International Energy Agency estimated that the volume of LIB waste from electric vehicles in 2019 alone was already 500,000 tons and predicted to rise to as much as 8 million tons in 2040 [4]. Hence, with the increasing consumption of lithium-ion batteries, landfill waste and environmental hazards, there is a need to recycle spent lithium-ion batteries. As of 2021, NMC 622 held 66% of the NMC battery market [5]. With the given trend, we have tailored the design of our battery recycling plant around the recycling of NMC 622 batteries. There is a market demand for Li_2CO_3 and mixed hydroxide precipitates containing $Ni(OH)_2$, $Mn(OH)_2$ and $Co(OH)_2$. The MHP is desired to have a low percentage of $Mn(OH)_2$. MHP and Li_2CO_3 is used to make more LIBs [6, 7].

2. Recent Process and Technological Development

The recent recycling processes in the industry can be generically divided into pre-processing and mechanical, pyrometallurgical, hydrometallurgical and direct recycling processes. Pre-processing is defined as any operation that does not modify the structure of the LIB cells. Mechanical processing is the application of various processes to release, categorize, and concentrate materials without changing their chemistry. These techniques operate based on relative differences in the physical properties of materials, such as density, shape, and size, and they generally occur before stages involving chemical reactions. After mechanical processing, the material obtained is refined by pyrometallurgy, hydrometallurgy, or a mixture of both [8]. Pyrometallurgy refers to operations at temperatures above 1200°C where valuable metals are extracted [9]. For example, roasting is one of the methods in pyrometallurgy that can be used to extract valuable metals from the cathode [10]. Hydrometallurgy involves the leaching of valuable elements from a solid matrix and their subsequent precipitation through modification of the solvent-phase chemistry [11]. For example, inorganic acids like SA, hydrochloric

acid and nitric acid are commonly used for leaching with reducing agents (e.g. H_2O_2) [12]. Direct recycling disassembles, breaks, and sorts the batteries before separating out targeted components via physical methods such as subcritical carbon dioxide extraction [13].

3. Current Methods' Analysis and Process Selection

The effectiveness of various LIB recycling procedures for the extraction of lithium (Li), nickel (Ni), cobalt (Co) was analysed via popular procedures used by companies, namely Accurec, LithoRec, and Retriev Technologies. Retriev Technologies focuses on a mechanical-hydrometallurgical process to recover metal oxides and Li_2CO_3. However, it is less desirable as these recovered metals are then used in other industries, and not to make more LIBs. Accurec and LithoRec were better references as they focused on recovering all the metals (Li, Ni & Co) using a mechanical-pyrometallurgical-hydrometallurgical process [8]. Therefore, a combination of the processes used by Accurec and LithoRec was adopted for the extraction of Li, Ni and Co from spent LIBs. However, we recognized the strong environmental impacts from energy consumption and gas emissions associated with pyrometallurgy [14]. Therefore, our project focused on hydrometallurgy methods to minimize these impacts and to find more eco-friendly solutions, eventually deciding on a mechanical, followed by hydrometallurgical process.

4. Process Description

Our plant was designed with a goal to process 5000 tons per year of lithium-ion batteries. The plant will operate at 70% capacity with respect to the active cathode material, and 4 batches of reactions will be conducted in a day. The processing capacity per batch (lithium battery) will be 5411.26 kg. Calculations for the processing capacity can be found in Appendix A. Operating at a lower level of capacity utilization ensures that the project has spare capacity to use to respond quickly to an increase in demand. This gives our project flexibility to scale up production without incurring significant costs or disruptions.

NMC 622 batteries received at our plant are assumed to have already been dismantled and do not contain peripherals, or electrolytes. The batteries will undergo a pre-treatment process that consists of four major stages: shredding and pyrolysis, crushing and sieving, electrostatic separation, and heavy liquid separation. During the first stage, 3516.02kg of cell materials (stream 1) will be shredded using SH-101 into 2cm strips and the effluent (stream 3) is subjected to pyrolysis with calcium oxide (stream 4, 18783.41kg) to remove the PVDF organic binder using H-101 (97.1% separation efficiency) [15]. This effluent (stream 6, 22235.63kg) is then cooled using E-101 and is then subsequently sieved using S-101, S-102, S-103 to separate the cell materials and impurities generated from pyrolysis. Since the amount of PVDF left is 0.001% of the subsequent streams, it is omitted from subsequent steps. The remaining cell materials (stream 23, 3391.74kg) will then be crushed using CR-101 and sieved using S-104 to separate the metals from the electrode materials [16, 17] (assumed to be 100% separation efficiency). Electrostatic separator, EL-101, will be used to separate stream 27, 1051.18kg of copper and aluminium (copper recovery: 68.6% and purity: 98.9%) [18]. 2340.56kg of mixture of active cathode material and anode material (graphite) (stream 33) will then be separated by heavy liquid separation using CE-101, CE-102, CE-103 [19] (assumed to be 100% separation efficiency). 1361.88kg of separated active cathode material, stream 41, will then be sent to a storage tank (atmospheric conditions) and subsequently be sent to a chemical reactor for hydrometallurgical processes.

Assumptions for mechanical (pre-treatment):

1. Batteries that arrive at our plant have been dismantled, and hence do not contain peripherals and electrolytes
2. Sieving time is linear and can be scaled up with respect to the dimension of the sieve
3. Separation efficiency for sieve is 100% (justified in Section 7.3)
4. Density obtained for heavy liquid and cell materials for Heavy liquid Separation is at room temperature, and there is negligible difference in density between 42°C and room temperature.
5. Separation efficiency for heavy liquid separation is 100% (justified in Section 7.5).

The hydrometallurgy process involves a two-step leaching process to extract LNMC from the crushed active cathode materials.

0.25M oxalic Acid (OA) entering at 13588.19 kg, 25°C and 1.01 bar will be required to leach out LNMC entering at 1361.88 kg, 25°C and 1.01 bar as metal oxalates in R-201 (operating at 80°C and 1.01 bar for 78 min) for first step leaching. This reactor will have a conversion rate of 99% [20] and the reactions occurring in R-201 are stated below (where '*m*' denotes Ni, Co and Mn).

$Li_2O + H_2C_2O_4 \rightarrow Li_2C_2O_4 + H_2O$ (1) $mO + H_2C_2O_4 \rightarrow mC_2O_4 + H_2O$ (2)

As only $Li_2C_2O_4$ is soluble in OA while NiC_2O_4, CoC_2O_4 and MnC_2O_4 are insoluble [20], we can separate lithium from the rest of the metals. The reaction mixture, 17244.46 kg, will be separated using centrifuge CE-201 into a liquid stream containing $Li_2C_2O_4$, leaving at 15621.75 kg, and a solid stream containing NMC oxalate precipitates, leaving at 1622.71 kg. The liquid stream will be heated to 103°C and 1.01 bar within flash drum V-201 to remove water. The water vapor stream leaving V-201 at 6584.57 kg will be split into two streams to be cooled by heat exchangers E-201 and E-202 to a temperature of 50°C and 1.01 bar. The liquid stream leaving V-201 at 9037.26 kg will be sent to R-204 (operating at 80°C and 1.01 bar) where K_2CO_3 will enter at 2496.00 kg to precipitate out Li as Li_2CO_3, with precipitation efficiency of 92% [21] and product purity of 97.8%.

$Li_2C_2O_4 + K_2CO_3 \rightarrow Li_2CO_3 + K_2C_2O_4$ (3)

The solid NMC stream, 1622.71kg, will be sent to R-202 to react with 32454.84 kg of 3.77M sulfuric acid (SA) at 60°C and 1.01 bar for 120 min for the second step leaching as seen in the reaction below (where '*m*' denotes Ni, Co and Mn) [20].

$mC_2O_4 + H_2SO_4 \rightarrow mSO_4 + H_2C_2O_4$ (4)

The resulting 34077.57 kg liquid mixture containing $MnSO_4$, $NiSO_4$ and $CoSO_4$ will be sent to R-203, where MgO powder will be added at 2947.00 kg to precipitate out NMC as $Ni(OH)_2$, $Co(OH)_2$ and $Mn(OH)_2$ at 50°C and 1.01 bar. This reaction will have a conversion rate of 90%, 95% and 50% respectively (where '*m*' denotes Ni, Co and Mn) [22] and product purity of 88.2% for $Ni(OH)_2$ and $Co(OH)_2$ combined.

$mSO_4 + MgO + H_2O \rightarrow m(OH)_2 + MgSO_4$ (5)

The exiting stream of 37797.57 kg will be sent to centrifuge CE-202, where the solid product stream will contain $m(OH)_2$ at 853.88 kg and the liquid waste stream will exit at 36943.69 kg to be collected in storage tank TK-202 for waste treatment.

The final products of this process are Li_2CO_3, and a mixed hydroxide precipitate (MHP) consisting of $Ni(OH)_2$, $Co(OH)_2$ and $Mn(OH)_2$. The liquid waste stream will be sent to TK-204 for waste treatment.

5. Reaction Kinetics Discussion

Assumptions and justifications for ASPEN Plus simulation:

Assumption 1: As the active cathode material particles could not be simulated in ASPEN Plus, individual metal compounds were used to simulate the active cathode material, as shown in Table 1. For leaching step 1, the literature [20] did not provide the reactions of the individual components, therefore the reactions were balanced based on stoichiometry as shown in Equations (1) and (2).

Table 1: Table of justification on simulated compounds

Original Component	Simulated Component	Reason
$LiNi_xCo_yMn_zO_2$	LiO (Lithium Oxide), CoO (Cobalt Oxide), NiO (Nickel Oxide), MnO (Lithium Manganese Oxide)	Could not be found in ASPEN Plus library
$LiPF_6$	$C_2H_3FN_2O_5$ (2-fluoro-2,2-dinitroethanol)	Similar molecular weight and boiling point to increase the accuracy when calculating energy required.

Assumption 2: From the literature, 1st step leaching reaction uses H_2O_2 as a reducing agent. However, our simulated active cathode material uses individual compounds which are in the form of oxides, there was no reaction involving OA using H_2O_2 as a reducing agent. Hence, H_2O_2 was not used for simulating the reactions.

Assumption 3: There were several steps taken to obtain the kinetic parameters for the various reactions.

1. The activation energy used for the individual reactions in the two leaching steps were based on literature values [20].

2. The first iteration of Arrhenius constant used was determined based on literature values. All the reactions were assumed to be second-order overall for leaching steps 1 and 2. To ensure the reaction duration and recovery rate matches the literature, two variables were varied, the Arrhenius constant and the exponents of the reactants.

Table 2: Table of recovery rates for various leaching steps

Leaching Step 1		Leaching Step 2	
Products	**Recovery Rates**	**Products**	**Recovery Rates**
$Li_2C_2O_4$	Experimental (99.2%), Simulation (99.90%)	$NiSO_4$	Experimental (99.9%), Simulation (99.9%)
NiC_2O_4	Experimental (99.983%), Simulation (99.99%)	$CoSO_4$	Experimental (100%), Simulation (100%)
CoC_2O_4	Experimental (99.971%), Simulation (99.95%)	$MnSO_4$	Experimental (99.2%), Simulation (100%)
MnC_2O_4	Experimental (99.44%), Simulation (99.95%)		

Assumption 4: Complete dissociation of OA and SA was assumed for the simulated leaching processes.

$$H_2C_2O_4 \rightarrow 2H^+ + {C_2O_4}^{2-} \quad (7) \qquad H_2SO_4 \rightarrow 2H^+ + {SO_4}^{2-} \quad (8)$$

Assumption 5: Power Law was assumed as the kinetic type for the simulated reactions, as the reactions mainly involve electrolytes and the reactions are irreversible.

6. Thermodynamic Model Validation

The leaching process was simulated using ASPEN Plus with the thermodynamic model ELECNRTL [23]. The simulated reactions consist of electrolyte solutions and include polar molecules in an aqueous environment. The main electrolytes in this paper are the acids $C_2H_2O_4$ and H_2SO_4. With reference to Carlson's Recommendations [24], ELECNRTL was the most suitable electrolyte property method [25] and the best option for the simulations carried out in this paper.

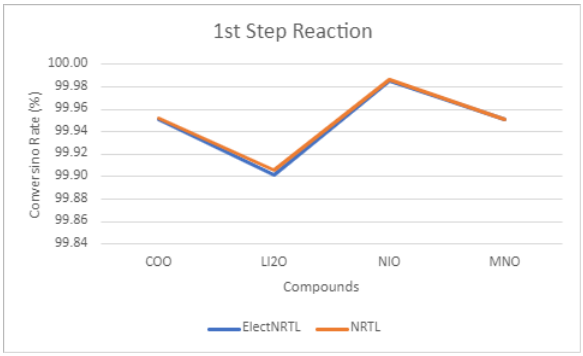

Figure 1: 1st step conversion (%) of salts in two different thermodynamic models

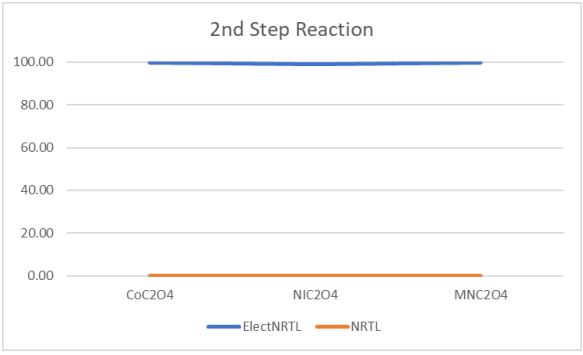

Figure 2: 2nd step conversion (%) of salts in two different thermodynamic models

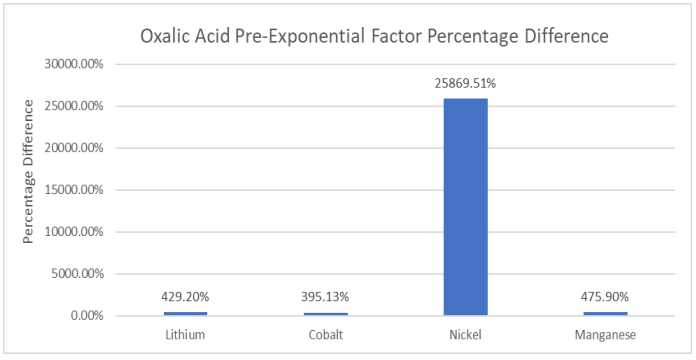

Figure 3: OA pre-exponential factor percentage difference

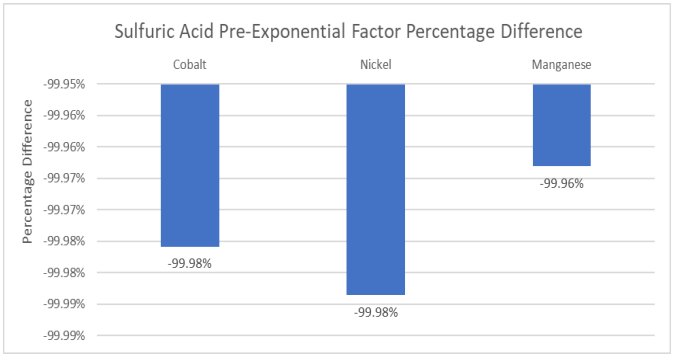

Figure 4: SA pre-exponential factor percentage difference

Figure 1 shows that there is little to no difference whereas Figure 2 shows a drastic difference between the two thermodynamic models. The is because the electrolyte parameters are available for SA in ASPEN Plus while they missing for oxalate acid.

Figure 3 & 4 show that there are big differences between the values provided in ASPEN Plus and literature value [20] for pre-exponential factor.

The values taken from literature had accounted for the diffusion and chemical kinetics whereas in ASPEN Plus, power law was used to mimic the reaction kinetics which only models chemical kinetics. Thus, the reason for the huge discrepancy between them. In addition, there is an anomaly for nickel in Figure 3 with a 25869% difference which suggest that power law is a bad model to describe nickel's reaction behaviour. Overall, power law is not advised to mimic the reaction behaviour for the 2 main leaching reaction.

7. Equipment Designing – Sizing and Material Analysis

7.1 Reduction Equipment

7.1.1. Shredder

Commercial Lvdao Machinery AT800 (L x W x H: 2.7m x 1m x 1.8m) is used to shred the feed stream (stream 1) into strips. According to manufacturer's specifications, the shredder has an estimated processing capacity of 1000kg/h [26]. This can be used to determine the duration needed to shred 3516kg of cell material, estimating at about 3.52h.

7.1.2. Hammer Mill

3391.74kg of cell materials in stream 23 (containing electrode materials, Cu and Al) will be broken down using a hammer mill that rotates at 3000 rad/min and crushed for 20s [16]. Due to the variances in their respective characteristics, this setting will cause the metals to be crushed into spherical particles that are approximately 0.25mm in diameter, and the electrode materials to be approximately 0.01mm in diameter [16].

7.2 Rotary Calciner & Rotary Cooler

The rotary calciner is utilized for simultaneous solid mixing and heating, making it an optimal choice for pyrolysis, where effective contact between calcium oxide (CaO) and electrodes is crucial for efficient fluoride capture [27]. CaO is used as a low temperature reaction medium to decompose PVDF. This reduces the energy requirements for the pyrolysis process and minimizes the risk of thermal degradation of cathode. CaO can also act as a capture reagent for the released fluoride from the thermal decomposition of PVDF, reducing hazardous byproducts released into the atmosphere [15]. Stainless steel was chosen as the material for construction due to its ability to withstand high temperatures and mechanical stresses associated with rotation [28].

Commercial rotary calciners typically range from 0.1m to 3m in diameter and 1m to 40m in length, with an L/D ratio of 5 to 20 [28, 29]. For the design of our rotary calciner, an L/D ratio of 16 and a diameter of 0.55m were selected. Parameters and heating duty calculations can be found in Table 3 respectively. The electric rotary calciner has an energy efficiency of 75% [2].

For the rotary cooler, it is sized to calciner's dimensions to ensure similar flowrate for smooth continuality. Similarly, stainless steel is used for the rotary cooler due to its high resistance for corrosion and can withstand constant exposure to water without corroding [30]. The rotary cooler has an energy efficiency of 47.75% [31].

7.3 Sieves

The sieves used are from Retsch Vibratory Sieve Shaker AS300 [32]. According to manufacturer's reports [33], a 0.2m by 0.2m sieve (area 0.04 m^2) can process 1.35kg of solid in 10 minutes. Using the assumption that the sieve time required is linear with respect to the sieve area, sample calculation of S-104 is shown. It is determined that sieve size of 1.67 m by 1.67 m is sufficient to finish processing 3395 kg of solids in 6 hours (1 batch).

$$\text{Surface area of sieve S} - 104 = 0.2 \times 0.2 = 0.04\text{m}^2$$

$$\text{Mass the sieve can process in 6h} = 1.35 \times 6 \times 6 = 48.6\text{kg}$$

$$\text{Factor used to handle 3395kg of materials in 6h} = \frac{3395}{48.6} = 69.86$$

$$\text{Area of the sieve} = 69.86 \text{ x } 0.04 = 2.79\text{m}^2$$

$$\text{Assuming the sieve is a square, length of the sieve} = 1.672\text{m}$$

Electrode materials and metals can be separated using a vibratory sieve [17] with perforations dimension of 0.25mm. The fraction of particles that will pass through the sieve and were under 0.25mm in size consisted of active materials [16]. It is noted that the separation efficiency of a sieve is primarily determined by the physical properties (particularly size) of the particles being sieved. Therefore, since the particle size is within the range of the sieve mesh, the separation efficiency of the sieve can be assumed close to 100%. A vibratory sieve's frequency and amplitude can be adjusted over a wide range, affecting separation efficiency as well. The ideal vibration frequency to separate particles smaller than 0.25 mm was 50 Hz, with an amplitude of 0.36 mm, and an interval period of 10s (at a minimum) [32].

7.4 Electrostatic Separator

Commercial VANER V-ES1200 electrostatic separator was used to separate copper and aluminium scraps. The electrostatic separator has an estimated processing capacity of 225kg/h [34], and this can be used to determine the duration needed to separate 1051.18kg of copper and aluminium, estimating at about 4.67h.

Based on the operation of the electrostatic separator, the recovery of copper is 68.6% and the purity of the stream is 98.9%. With this information, the purity of copper and aluminium stream can be calculated.

$\text{Mass of copper} = 693.88\text{kg}$
$\text{Mass of copper in copper stream} = 693.88 \times 0.686 = 476.00\text{ kg}$
$\text{Mass of copper stream} = 476.00 \div 0.989 = 481.30\text{kg}$
$\text{Mass of aluminium in copper stream} = 481.30 - 476.00 = 5.29\text{kg}$

$\text{Mass of aluminium} = 357.30\text{kg}$
$\text{Mass of aluminium in aluminium stream} = 357.30 - 5.30 = 352.00\text{kg}$
$\text{Mass of copper in aluminium stream} = 693.88 - 476.00 = 217.88\text{kg}$
$\text{Recovery of aluminium} = 352.00 \div 357.30 = 98.5\%$
$\text{Purity of aluminium stream} = 352.00 \div (357.30 + 217.88) = 61.8\%$

7.5 Centrifuges

Centrifuge was chosen as it was the most efficient equipment for solid-liquid separations. Other separation equipment options include thickeners, clarifiers, filters and hydrocyclones. However, these options were either too time-consuming or expensive [35].

7.5.1. Industrial and Decanter Centrifuge

Industrial and decanter centrifuge was used for heavy liquid separation in the pre-treatment process [19]. Volumes of the products in the respective streams are required to size the centrifuges. The volume can be calculated using values obtained from the mass balance and the density of the component. Taking into consideration the heavy liquid volume and the assumption that a centrifuge is 75% filled [36], volume sample calculation for CE-101 is shown in below. The height and diameter of a centrifuge are inversely proportional. For a constant centrifuge volume, increase in height will result in a reduction of its diameter. Since the equipment cost of a centrifuge is dominantly dependent on its diameter [35], a smaller diameter will result in a cost-effective design. Since the equipment cost of a centrifuge is dominantly dependent on its diameter [35], a smaller diameter will result in a cost-effective design. With the maximum height of a centrifuge in application set at 2m [37], the diameter of the centrifuge can thus be determined.

Density of active cathode is 4700kg/m3, density of graphite is 2300kg/m3 [38]

Table 3: Physical Properties of Components in Black Mass

Components	Mass Flow	Density (kg/ m^3)	Volume (m^3)
Li2O	539.7063212	4700	0.290
NiO	498.2335613		
CoO	167.5723676		
MnO	156.3635136		
Graphite	978.6863854	2230	0.445

$Total\ volume\ of\ black\ mass = 0.290 + 0.445 = 0.735m^3$

For every 15g of solid, 25ml of separating liquid is used [39]. Hence, the amount of heavy liquid required for 2341kg of solids can be calculated as follows.

$\text{Volume of heavy liquid} = \left(\frac{2341\text{kg}}{0.015\text{kg}} \times 25\text{ml}\right) = 3900936\text{ml} = 3.90\text{m}^3 \approx 4\text{m}^3$

$\text{Since the volume of heavy liquid is } 4\text{m}^3, \text{ volume of centrifuge required} = 4.735\text{m}^3$

Assume centrifuge is 75% full [36],

$$\text{Volume of centrifuge} = 4.735 \div 0.75 = 6.31\text{m}^3$$

For a constant centrifuge volume, increasing its height will result in a reduction of its diameter. Since the cost of a centrifuge is determined by its [35], a smaller diameter will lead to a more cost-effective design.

The maximum height of a centrifuge in application is 2m [37], hence by setting the height at 2m, the diameter of centrifuge is given to be: $D\text{iameter} = 2 \times \sqrt{(6.31 \div \pi \div 2)} = 2.005\text{m}$

The heavy liquid separation efficiency is heavily dependent on the physical properties, specifically density difference, of the particles being separated. Since the heavier (active cathode NMC622) particles will sink to the bottom while the lighter (graphite) particles will float on top of the heavy liquid, separation efficiency can be assumed to be 100% for industrial centrifuge. In addition, separation efficiency of decanter centrifuge can also be assumed to be 100% [40].

Sodium Polytungstate (SPT) is a heavy liquid widely used in mineral industries due to its thermal and chemical stability and low toxicity, making it a suitable option for separating components in spent lithium-ion batteries (LIBs) [41]. Despite its high initial investment, SPT is reusable to ensure continuity and reduces waste [19].

7.5.2. Horizontal Auto-batch Centrifuge

Horizontal auto-batch centrifuge was used for hydrometallurgical processes. The size is dependent on solid mass flow. The solid flow for our processes was low at 1-2ton/h. However, the overall stream flow was much higher at 13-41ton/h. To account for the higher overall flowrate, the maximum diameter of a centrifuge was selected. Thus, a 43in centrifuge diameter was selected [35]. The material used was stainless steel as it can handle OA and very dilute SA [42].

7.6. Reactor

7.6.1. Sizing

There is a total of four agitated reactors in this process. For these reactors, the torispherical top and bottom head type was selected due to its ability to withstand pressures up to 20 bar. It is also the cheapest to create and manufacture [43]. The sizing of each reactor was determined based on the volumetric load of the reactions taking place. Between the volume of the reactants and the products, the larger volume was taken as the volumetric load. For agitated vessels, this volume should be 80% of the total reactor volume, to prevent leakage and for other safety reasons [43] . Using the first stage leaching reactor as example, the total volume of reactants and products are 14.85m^3 and 16.37m^3 respectively. Taking 16.37m^3 to be 80% of the reactor volume required, the reactor volume required is calculated to be 20.46m^3. Using this volume and Aspen Plus reactor sizing tool, the tangent-to-tangent length (L) and diameter (D) of the reactor can be determined, constrained by the rule of thumb stating that aspect ratios (L/D) of pressured vessels should fall in the range between 1.0-1.5 [43]. The values of L and D calculated for the aforementioned reactor is 3m and 2.69m respectively. The same calculations are repeated for the other three reactors and the dimensions of all reactors are thus obtained.

7.6.2. Material Selection

The two-step leaching process involves the handling of SA and OA. To prevent corrosion and ensure the safety of plant operations, the choice of materials for the reactors is paramount. For the 1st leaching and Li precipitation reactions, the reactor contains the corrosive material OA. Stainless steel 316 is the industrial standard material of construction for pressure vessels that is compatible with our process. It is excellent in handling OA of below 10wt% at room temperature [42]. By extension, it would be a material capable of supporting the reactions, which only contain below 2.2wt% OA. Stainless steel 304, its cheaper counterpart, was shown to be less corrosive resistant to OA than stainless steel 316 [44]. This disparity is magnified when the temperature of reaction is higher, at 80^{o}C. To mitigate vessel corrosion for safety and economic reasons, stainless steel 316 will be the choice of material for the first stage leaching and Li precipitation reactors.

For the second stage leaching and NMC precipitation reactions, the reactor contains SA, which is highly corrosive in nature. For both reactions, SA is above 20wt%. Stainless steel 316 is no longer able to handle the reaction [42] and an alloy with higher corrosion

resistance had to be chosen. The Carpenter 20 CB-3 (Alloy 20) is the next cheapest alternative that can withstand 30wt% SA at temperatures below 70°C [31]. The second stage leaching reactor contains the highest concentration of SA, at 27% at 60°C. Alloy 20 is able to handle this reaction and thus it will be able to handle the NMC precipitation reaction as well. Thus, Alloy 20 will be the choice of material for the second stage leaching and NMC precipitation reactors.

7.7. Heat Exchangers (E-201, E-202)

In the designing of the shell and tube heat exchangers, an iterative method was used to obtain an overall heat transfer coefficient that had a value that was less than 5% difference from the calculated value in the previously iterated step. The heat exchanger sizing that corresponds to the final iterated value would then be used for the calculation of the equipment cost.

Table 4: Justification for TEMA Type [45]

TEMA type	Justification
A	• Cheaper header type to reduce capital cost • As the process operates under atmospheric conditions, this header type can be used • Tube interior can be accessed without affecting the pipe work
E	• Common shell type in the industry.
L	• Due to the low fouling nature for the fluid in the shell, the lack of access to the exterior of the tube can be tolerated. Regular chemical cleaning can be used during maintenance to reduce fouling. • Access to interior of tube is possible without removing any pipework.

A total of two shell and tube heat exchangers (E-201 and E-202) were used in the process, whereby the heat exchangers were used in parallel to condense the vapour stream (steam) exiting the flash drum (V-201), from 103°C to 50°C. Two similar heat exchangers were used in parallel by splitting the vapour stream equally. This was due to the pressure drop generated in the heat exchanger for the vapour stream (if stream is not split) for only one heat exchanger was above the heuristics given of 1.5psi [43]. The vapour stream would be located in the shell side, whereas the cooling water stream would be located in the tube side, this was because the shell will be able to tolerate the two-phase flow as steam was condensed in the heat exchanger [46]. Based on the process requirement, the TEMA type for the shell and tube heat exchanger was chosen to be A-E-L and the justification was shown in Table 4. Triangular pitch of the tubes were used as it would result in better heat transfer as compared to a square pitch, furthermore as only steam is used in the shell side, regular mechanical cleaning on the shell side is not required, making triangular pitch a better option [35]. The baffle type used for both the heat exchangers were vertical single segmental baffle as two-phase flow is present in the shell.

As both the vapour stream and cooling water stream mainly contains water, the material of construction for both the shell and tube can be carbon steel.

A sample calculation is shown in Table 5 to obtain the equipment sizing.

Table 5: Heat Exchanger Sample Calculations[47, 48]

A: Steam – S (Shell Side)			**B: Cooling Water – CW (Tube Side)**		
Inlet Temperature, T_1	°C	103	Inlet Temperature, t_1	°C	32
Outlet Temperature, T_2	°C	50	Outlet Temperature, t_2	°C	49
Mass Flowrate, $\dot{m}_S$	kg/s	$9.23\text{x}10^{-1}$	Pressure, P_{CW}	bar	1.01
Pressure, P_S	bar	1.01	Average Heat Capacity, $C_{p,CW}$	kJ/kg.K	4.18
Heat Capacity (Vapour), $C_{p,S,v}$	kJ/kg.K	1.91	Average Thermal Conductivity, k_{CW}	kW/m.K	$6.28\text{x}10^{-4}$
Heat Capacity (Liquid), $C_{p,S,l}$	kJ/kg.K	4.18	Average Density, ρ_{CW}	kg/m^3	991.83
Thermal Conductivity (Vapour), $k_{S,v}$	kW/m.K	$2.44\text{x}10^{-5}$	Average Viscosity, μ_{CW}	N.s/m^2	$6.78\text{x}10^{-4}$
Thermal Conductivity (Liquid), $k_{S,l}$	kW/m.K	$6.41\text{x}10^{-4}$	Mass Flowrate, $\dot{m}_{CW} = \frac{Q}{C_{p,CW^*}(t_2-t_1)}$	kg/s	32.15
Density (Vapour), $\rho_{S,v}$	kg/m^3	$5.88\text{x}10^{-1}$	Volumetric Flowrate, $\dot{V}_{CW} = \frac{\dot{m}_{CW}}{\rho_{CW}}$	m^3/s	$3.24\text{x}10^{-2}$
Density (Liquid), $\rho_{S,l}$	kg/m^3	988.08	**C: LMTD Calculation**		
Viscosity (Vapour), $\mu_{S,v}$	N.s/m^2	$1.25\text{x}10^{-5}$	$LMTD_{ideal} = \frac{((T_1-t_2)-(T_2-t_1))}{\ln\left(\frac{(T_1-t_2)}{(T_2-t_1)}\right)}$	°C	32.77
Viscosity (Liquid), $\mu_{S,l}$	N.s/m^2	$5.60\text{x}10^{-4}$	$R = \frac{T_1-T_2}{t_2-t_1}$	-	3.12
Change in Enthalpy, $\Delta H_{S,v}$	kJ/kg	2262.98	$S = \frac{t_2-t_1}{T_1-t_1}$	-	$2.39\text{x}10^{-1}$
Outlet Vapour Fraction	-	0	Correction Factor, $F_T = \frac{\sqrt{R^2+1}\ln\left[\frac{1-S}{1-RS}\right]}{(R-1)\ln\left[\frac{2-S\left(R+1-\sqrt{R^2+1}\right)}{2-S\left(R+1+\sqrt{R^2+1}\right)}\right]}$	-	$8.26\text{x}10^{-1}$
Heat Duty, $Q = \dot{m}_S\Delta H_{S,v} + \dot{m}_S C_{p,S,l}(100°C - T_2)$	kW	2282.48			
D: First Iteration Calculation (Tube Side)					

Estimated Overall Heat Transfer Coefficient, U_O	kW/m^2.K	1.05	$LMTD_{corrected} = LMTD_{ideal}F_T$	ºC	27.08
Area Required, $A = \frac{Q}{U_O LMTD_{corrected}}$	m^2	80.29	**E: First Iteration Calculation (Shell Side)**		
Tube Length, L_t	m	6.10	Tube Pitch, $p_t = 1.25d_o$	m	3.18x10^{-2}
Surface Area of one tube, $A_{tube} = \pi d_o L_t$	m^2	4.86x10^{-1}	K_1	-	0.249
Number of Tubes, $N_t = \frac{A}{A_{tube}}$	-	166	n_1	-	2.207
Tube Inner Diameter, $d_i = d_o - Tube\ Thickness \times 2$	m	2.21x10^{-2}	Bundle Diameter, $D_b = d_o\left(\frac{N_t}{K_1}\right)^{\frac{1}{n_1}}$	m	4.83x10^{-1}
Cross-sectional Area of one tube, $A_{cross} = \frac{\pi {d_i}^2}{4}$	m^2	3.84x10^{-4}	No. of tubes in central row, $N_{cr} = \frac{D_b}{p_t}$	-	15.23
Number of Tube Pass, N_p	-	2	No. of tubes in vertical row, $N_r = \frac{2}{3}N_{cr}$	-	10.15
Tube Equivalent Diameter, $d_e = \frac{4A_{cross}}{\pi d_i}$	m	2.21x10^{-2}	Shell-bundle Clearance, D_c	m	1.3x10^{-1}
Tube Side Velocity, $u_{tube} = \frac{\dot{V}_{CW}}{A_{cross}\left(\frac{N_t}{N_p}\right)}$	m/s	1.02	Shell Inner Diameter, $D_i = D_b + D_c$	m	4.96x10^{-1}
Reynolds Number, $Re = \frac{\rho_{CW} u_{tube} d_e}{\mu_{CW}}$	-	3.29x10^4	Tube Loading, $\Gamma_h = \frac{\dot{m}_S}{LN_r}$	kg/m.s	9.12x10^{-4}
Prandtl Number, $Pr = \frac{C_{p,CW}\mu_{CW}}{k_{CW}}$	-	2.25	Shell Side Heat Transfer Coefficient, $h_o = 0.95k_{S,l}\left[\frac{\rho_{S,l}(\rho_{S,l}-\rho_{S,v})g}{\mu_{S,l}\Gamma_h}\right]^{\frac{1}{3}} N_r^{-\frac{1}{6}}$	kW/m^2.K	10.99
Tube Side Heat Transfer Factor, j_h	-	3.5x10^{-3}	Steam Fouling Factor, h_{od}	kW/m^2.K	4
Tube Side Heat Transfer Coefficient, $h_i = \frac{j_h Re Pr^{0.33} k_{CW}}{d_e}$ Error! Bookmark not defined.	kW/m^2.K	4.28	Baffle Spacing, L_s	m	4.96x10^{-1}
Cooling Water Fouling Factor, h_{id}		4	Cross-flow Area, $A_{cross-flow} = \frac{D_i L_s (p_t - d_o)}{p_t}$	m^2	4.93x10^{-2}
Tube Side Friction Factor, $j_{f,t}$	-	3.5x10^{-3}	Shell Side Velocity, $u_{shell} = \frac{\dot{m}_S}{A_{cross-flow}\rho_{S,v}}$	m/s	
Tube Side Pressure Drop, $\Delta P_t = N_p\left[8j_{f,t}\left(\frac{L_t}{d_i}\right) + 2.5\right]\left(\frac{\rho_{CW}u_{tube}^2}{2}\right)$	Pa	1.05x10^4	Shell Equivalent Diameter, $D_e = \frac{1.1\left(p_t^2 - 0.917 d_o^2\right)}{d_o}$	m	1.80x10^{-2}
F: Overall Calculation			Reynolds Number, $Re = \frac{\rho_{S,v} u_{shell} D_e}{\mu_{S,v}}$	-	2.71x10^4
Tube Material Thermal Conductivity, k_w	kW/m.K	3.6x10^{-2}	Shell Side Friction Factor, $j_{f,s}$	-	3.5x10^{-2}
Calculated Overall Heat Transfer Coefficient, $U_{O,c} = \frac{1}{\frac{1}{h_o} + \frac{1}{h_{od}} + \frac{d_o \ln\left(\frac{d_o}{d_i}\right)}{2k_w} + \frac{d_o}{d_i h_{id}} + \frac{d_o}{d_i h_i}}$	kW/m^2.K	1.06	Shell Side Pressure Drop, $\Delta P_s = 0.5\left[8j_{f,s}\left(\frac{D_i}{D_e}\right)\left(\frac{L_t}{L_s}\right)\right]\left(\frac{\rho_{S,v}u_{shell}^2}{2}\right)$	Pa	1.41x10^4
Difference in U_o	%	0.70			

The stream data shown in Section A and B for Table 5 were obtained using ASPEN Plus. The corrected LMTD was then calculated as shown in Section C as a 1-2 shell and tube heat exchanger was chosen. This was followed by the calculations for the tube side (Section D) to obtain the heat transfer coefficient (h_i) and pressure drop (ΔP_t). Next, the shell side heat transfer coefficient (h_o) and pressure drop (ΔP_s) was determined based on Section E. Section F shows the computation of the calculated overall heat transfer coefficient ($U_{O,c}$) and if the percentage difference between the estimated U_o and $U_{o,c}$ exceeds $\pm 5\%$, another iteration would have to be done.

7.8. Agitator

The reactors contain slurries of low viscosity, thus the pitched blade turbine is selected [43]. Based on the reference range of 0.5 – 10 Horsepower (Hp)/1000Gallons (Gal), 10Hp/1000Gal was chosen as it is best for suspension of solid particles [43]. The turbine speed used is 320 rounds per minute (rpm) based on the reference range of 37 to 320 rpm [35]. As the higher Hp is used from the reference range, the higher rpm is also selected accordingly. The number of blades does not have much influence on the mixing effectiveness for slurries with low solid concentrations, so 4 blades was chosen as it has a lower power number [49]. The turbine diameter was determined following the tank diameter to turbine diameter ratio of 3:1. The material used is stainless steel for the 1st step leaching process and lithium precipitation. For the 2nd step leaching and NMC

precipitation, Monel was used instead as it more suitable that stainless steel for processes containing SA [50].

The flow in all the reactors are fully turbulent based on Reynolds number, thus the power number used is 1.27 [43]. Power is calculated following the equation $P = \frac{N_p \rho N^3 D^5}{g_c}$, where g_c is 1m/s^2.

7.9. Flash drum

7.9.1. Sizing

The vertical separator was chosen for the process as it is preferred for conducting separations with a high vapor/liquid ratio (>750) [51]. The vapor/liquid ratio for the separation process is ~1200, well over the benchmark. Additionally, it reduces the land area occupied by the vessel, saving land costs and suitable for off-shore operations. Demister pads were integrated in the vertical separator design to reduce the entrainment of liquid OA droplets, potentially causing downstream corrosion, and loss of precious product lithium oxalate, which is soluble in water. An inlet diverter was also included in the design to induce primary separation of liquid droplets entrained in the vapor. The length and diameter of the separator was determined by a set of calculations [52] tabulated in Table 6 below.

Table 6: Calculation of length and diameter of flash drum

Parameters	Unit	Value	Parameters	Unit	Value
Pressure, P (obtained from Aspen Plus)	psia	14.70 (101325 Pa)	Surge volume, $V_S = T_S * Q_L$	ft^3	27.45 (0.78 m^3)
Terminal velocity constant, $K = 0.1821 + 0.0029 * (P) + 0.046 * \ln(P)$ (case for including mist eliminator)	ft/s	0.35 (0.11 m/s)	Low Liquid Level height, H_{LLL} (Vessel diameter between 4 and 6 ft, flashing pressure below 300 psia)	ft	1.25 (0.38 m)
Liquid density, ρ_L (obtained from ASPEN Plus)	lb/ft^3	60.43 (967.91 kg/m^3)	Holdup height, H_H $H_H = \frac{V_H}{\left(\frac{\pi}{4}\right)D^2}$	ft	3.45 (0.38 m)
Vapor density, ρ_V (obtained from ASPEN Plus)	lb/ft^3	$3.67x10^{-2}$ ($0.59\ kg/m^3$)	Surge height, H_S $H_S = \frac{V_S}{\left(\frac{\pi}{4}\right)D^2}$	ft	1.73 (0.53 m)
Terminal velocity, U_T $U_T = K\sqrt{\frac{\rho_L - \rho_V}{\rho_V}}$ (Souders-Broun equation)	ft/s	14.13 (4.31 m/s)	Mixture volumetric flow, Q_M $Q_M = Q_V + Q_L$	ft^3/s	96.37 ($2.73\ m^3/s$)
Vapor volumetric flow, Q_V	ft^3/s	96.28 ($2.72\ m^3/s$)	Mixture liquid fraction, λ $\lambda = \frac{Q_L}{Q_V + Q_L}$	-	$9.49x10^{-4}$
Vapor disengagement diameter, D_{VD} $D_{VD} = \sqrt{\frac{4 * Q_V}{\pi * 0.75 * U_T}}$ (assuming $U_V = 0.75U_T$ for conservative estimate)	ft	3.40 (1.03 m)	Mixture density, ρ_M $\rho_M = \rho_L\lambda + \rho_V(1-\lambda)$	lb/ft^3	$9.40x10^{-2}$ ($1.51 kg/m^3$)
Vessel diameter, D $D_{VD} = 43.814\ in$, $D = (43.814 + 6) in$, $D \approx 54\ in = 4.5ft$ (adding 6 inches to accommodate for the support ring of the mist eliminator and rounding off to the next 6-inch increment)	ft	4.5 (1.37 m)	Nozzle diameter, d_N $d_N = \sqrt{\frac{4Q_M}{\left(\frac{\pi * 60}{\sqrt{\rho_M}}\right)}}$	ft	0.39 (0.12 m)
Liquid volumetric flow, Q_L	ft^3/min	5.49 ($2.59x10^{-3}\ m^3/s$)	Low liquid level to inlet nozzle centreline height, H_{LIN} $H_{LIN} = (12 + d_N)\ in$, $H_{LIN} = 1.480ft$	ft	1.39 (0.42 m)
Holdup time, T_H (assuming unit feed drum)	min	10 (600 s)	Disengagement height, H_D $H_D = 24 + 0.5d_N$ (case for including mist eliminator)	ft	2.20 (0.67 m)
Holdup volume, V_H $V_H = T_H Q_L$	ft^3	54.89 ($1.55\ m^3$)	Mist eliminator to top tank height, H_{ME} $H_{ME} = \frac{6in}{\left(\frac{12in}{ft}\right)} + 1ft$	ft	1.5 (0.46 m)
Surge time, T_S (assuming unit feed drum)	min	5 (300 s)	Total vertical separator height, H_T $H_T = H_{LLL} + H_H + H_S + H_{LIN} + H_D + H_{ME}$	ft	11.52 (3.51 m)

7.9.2. Material Selection

Similar to the first stage leaching reactor, the liquid component in the flash drum contains the corrosive material OA. Stainless steel 316 is the industrial standard material of construction for pressure vessels that is compatible with our process. It is excellent in handling OA of below 10wt% at room temperature [42]. By extension, it would be a material capable of supporting the separation, which only contains 0.4wt% OA. Stainless steel 304, its cheaper counterpart, was shown to be less corrosive resistant to OA than stainless steel 316 [44]. This disparity is magnified when the temperature of flashing is at 100°C. To mitigate vessel corrosion for safety and economic reasons, stainless steel 316 will be the choice of material for the flash drum.

7.10 Centrifugal Pump

The general process stream is a slurry type, so the viscosity is higher than water. But the viscosity is likely to be below 150cP and is not a shear sensitive or non-Newtonian working fluid, so we will not use positive displacement pumps. Centrifugal pumps are the most common, applicable, efficient and affordable, hence centrifugal pumps were chosen [53].

8. Costing and Economics

8.1. Costing

8.1.1. Equipment Cost Summary

This process's overall bare-module cost is USD 86,185,697.84. The overall utility and raw material cost have also been summarized in the tables below in USD thousands. This includes the cooling water (CW) at 32℃ and low-pressure steam (LPS) used.

Table 7: Table of Utility Costs

Utilities	Unit	Unit Cost (USD)	Yearly Cost (USD k)
CW [54]	m^3	1.19	1,333.18
Electricity[55]	MWh	167.58	630.05
LPS [56]	ton	120.68	5,743.29
		Total Annual Utility cost:	7,706.52

Table 8: Table of Raw Material Costs

Raw Material Cost			
Chemical	**Mass needed per batch (kg)**	**Unit price per kg (USD)**	**Cost per year (USD k)**
$C_2H_2O_4$ [57]	1,226.17	0.73	1,179.92
CaO [58]	18,724.50	12.16×10^{-3}	300.55
Disposed LiNMC battery [59]	4,127.05	3.57	19,448.33
H_2O [54]	35,765.19	1.58×10^{-3}	56.04
H_2SO_4 [60]	8,455.75	0.85	9,487.35
K_2CO_3 [61]	2,321.86	0.61	1,869.56
MgO [62]	2,947.00	0.18	700.21
SPT (Heavy Liquid) [63]	11,600.00	170.00	131.47
		Total:	**31,862.04**

8.1.2. Equipment Cost

To calculate the estimated total capital investment required, Lang and Guthrie method was used [35]. The free-on-board base purchase cost of each equipment is shown below, where we have accounted for (a) the different materials of each equipment and (b) the effects of inflation. As our designed process will operate at 1 atm, there is no need to apply a pressure correction factor. The steps taken are as follows, for (a), a materials-of-construction factor, F_M, is applied to account for the difference between the actual material and the assumed carbon steel base material. For (b), a ratio of the inflation index (CEPCI) is used to correct for inflation. As such, the general formula $C_{BM} = C_P \times F_{BM}$. The table below shows the breakdown of the calculations for C_{BM}.

Some equipment used cannot be estimated using the Lang and Guthrie method, hence commercial purchases were done (Table 9).

Table 9: Tables of Equipment Cost Calculations

Equipment number	Free-on-Board Purchase Cost (Cp) Calculation					Bare Module Cost (CBM) Calculations		
	Equation	Diameter (m)	Cp, base (USD k)	Ratio of CEPCI index	Cp (USD k)	Material	BM Factor (FBM)	Cbm (USD k)
CE-101	$Cp = 6180D^{0.94}$	2.00	375.30	1.44	540.31	Stainless Steel	2.03	1096.82
CE-102	$Cp = 2440D^{1.11}$	1.39	208.07		299.55			608.09
CE-103		1.44	215.77		310.65			630.61
CE-201	$Cp = 2440D^{1.11}$	1.09	158.69	1.44	228.46	Stainless Steel	2.03	463.77
CE-202								
CE-203								

Equipment number	Free-on-Board Purchase Cost (Cp) Calculation					Bare Module Cost (CBM) Calculations		
	Equation	Area (m^2)	Cp, base (USD k)	Ratio of CEPCI index	Cp (USD k)	Material	BM Factor (FBM)	Cbm (USD k)
S-101	$Cp = 1588\ A^{0.71}$	6.18	31.26	1.44	45.00	Carbon Steel	1.73	77.85
S-102		6.18	31.26		45.00			77.85
S-103		6.18	31.26		45.00			77.85
S-104		3.34	20.22		29.11			50.35

Equipment number	Free-on-Board Purchase Cost (Cp) Calculation					Bare Module Cost (CBM) Calculations		
	Equation	Volume (m^3)	Cp, base (USD k)	Ratio of CEPCI index	Cp (USD k)	Material	BM Factor (FBM)	Cbm (USD k)
TK-101	$Cp = 265V^{0.513}$	5.07	10.65	1.44	15.33	Carbon Steel	4.16	63.78
TK-102		33.01	27.85		40.09			166.77
TK-103		28.29	25.73		37.04			154.08
TK-104		4.72	10.27		14.78			61.49
TK-105		4.72	10.27		14.78			61.49
TK-106		1.05	4.74		6.83			28.40
TK-107		0.77	4.06		5.84			24.30
TK-108		0.27	2.38		3.43			14.28
TK-109		3.67	9.03		13.00			54.06
TK-110		2.22	6.98		10.05			41.80
TK-111		20	21.53		31.00			128.96
TK-112		1.45	5.60		8.06			33.55
TK-201		0.26	5.27		7.58			31.53
TK-202		36.22	66.68		96.00			399.35
TK-203		6.73	28.12		40.48			168.39
TK-204		9.68	33.89		48.80			202.99
TK-205		0.54	7.72		11.12			46.25

Equipment number	Free-on-Board Purchase Cost (Cp) Calculation					Bare Module Cost (CBM) Calculations		
	Equation	Flow rate (m^3/h)	Cp, base (USD k)	Ratio of CEPCI index	Cp (USD k)	Material	BM Factor (FBM)	Cbm (USD k)
CR-101	$Cp = 4310\ W^{0.78}$	463.66	2.55	1.44	15.00	-	2.3	8.45

Equipment number	Free-on-Board Purchase Cost (Cp) Calculation								Bare Module Cost (CBM) Calculations			
	Equation	Type factor, Ft	H (m)	S $(m^3/s)\cdot(m^{0.5})$	C_B (USD k)	Cp, base (USD k)	Ratio of CEPCI index	Cp (USD k)	Material	Materials-of-construction factors, Fm	BM Factor (FBM)	Cbm (USD k)
P-201	$C_p = F_T F_M C_B$	1.00	0.46	2.58×10^{-3}	6.89	20.32	1.44	29.25	Hastelloy C	2.95	3.30	96.52
P-202			0.26	3.62×10^{-3}	6.16	18.16		26.14				86.28
P-203			0.31	4.63×10^{-3}	5.70	16.81		24.20				79.87
P-204			0.48	1.81×10^{-3}	8.37	24.69		35.55				117.30

Agitator in Reactor number	Free-on-Board Purchase Cost (Cp) Calculation					Bare Module Cost (CBM) Calculations			
	Equation	Size factor, Hp	Cp, base (USD k)	Ratio of CEPCI index	Cp (USD k)	Material	Materials-of-construction factors, Fm	BM Factor (FBM)	Cbm (USD k)
R-201	$C_p = 4105\,H_p^{0.57}$	43.24	35.14	1.44	101.17	Stainless Steel	2.00	1.38	139.61
R-202		60.00	42.35		164.62	Monel	2.70		227.18
R-203		60.00	42.35		164.62				227.18
R-204		27.67	27.24		78.44	Stainless Steel	2.00		108.24

Equipment number	Free-on-Board Purchase Cost (Cp) Calculation						Bare Module Cost (CBM) Calculations			
	Equation	C_{pL} (USD k)	Cv (USD k)	Ratio of CEPCI index	Cp (USD k)	$C_{p,jacketed}$ (USD k)	Material	Materials-of-construction factors, Fm	BM Factor (FBM)	Cbm (USD k)
R-201	$C_p = F_M C_V + C_{pL}$	9.89	507.11	1.44	1,547.40	1,856.88	Stainless Steel 316	2.10	4.16	7,724.62
R-202		13.89	839.80		3,888.90	4,666.68	Carpenter 20CB-3	3.20		19,413.39
R-203		15.99	1,003.48		4,644.59	5,573.50		3.20		23,185.77
R-204		8.87	400.00		1,222.11	1,466.54	Stainless Steel 316	2.10		6,100.79
V-201		7.02	217.66		668.15	-				2,779.48

Table 10: Individual Commercial Equipment Cost Breakdown

Equipment number	Commercial Purchase Cost (USD k)
E-101 [64]	9.73

EL-101 [65]	6.60
H-101 [66]	67.50
SH-101 [67]	15.00

Purchase cost of E-101 and H-101 are estimated, method of estimation can be found in Appendix B

8.1.3. Plant Utility Cost

Most of the equipment use LPS and CW to heat and cool the process streams as they are the cheapest options.

Table 11: Individual Equipment Utility Breakdown

Reactor										Flash Drum
Equipment	R-201		R-202		R-203		R-204			V-201
Function	heater	cooler	heater	heater	cooler	heater	cooler	heater	cooler	heater
Heat load per batch (kJ)	3.17×10^{6}	-3.40×10^{7}	2.89×10^{6}	1.21×10^{7}	-8.05×10^{5}	2.64×10^{7}	-6.50×10^{5}	2.12×10^{7}	-9.89×10^{5}	1.65×10^{7}
Utility Type	LPS	CW	LPS	LPS	CW	LPS	CW	LPS	CW	LPS
Utility per batch (kg)	4,531.22	478,416.56	4,041.54	5,252.03	43,781.49	11,474.18	35,502.10	9,194.54	48,227.36	1,813.39
Cost per year (USD k)	721.83	883.73	644.00	1,006.81	68.48	1,762.34	55.53	1,473.08	75.44	288.88

Agitator				
Equipment	R-201	R-202	R-203	R-204
Utility Type	Suspension of solid particles			
Revolutions per sec	5.33			
Fluid Density (kg/m3)	1.07×10^{9}	1.28×10^{9}	1.17×10^{9}	1.19×10^{9}
Viscosity (Ns/m2)	4.25×10^{-4}	1.06×10^{-3}	1.02×10^{-3}	6.09×10^{-4}
Reynolds Number	9.56×10^{6}	6.63×10^{6}	7.80×10^{6}	5.53×10^{6}
Power Number (Np)	1.27			
Utility Type	Electricity			
Utility per batch (MWh)	0.13	0.88	0.41	0.05
Cost per year (USD k)	39.59	192.90	90.29	10.38

Heater		
Equipment	H-101	
Type	Rotary Calciner	
Area (m^2)	15.75	
Material	Stainless Steel	
Function	Heating	Rotation
Utility Type	Electricity	
Utility per batch (MWh)	0.3300	1.9×10^{-2}
Cost per year (USD k)	73.69	4.31
Total Cost per year (USD k)	78.01	

Cooler		
Equipment	E-101	
Type	Rotary Cooler	
Area (m^2)	15.75	
Material	Stainless Steel	
Utility Type	CW (m^3)	Electricity (MWh)
Utility per batch	16.20	1.9×10^{-2}
Cost per year (USD k)	25.44	4.31
Total Cost per year (USD k)	29.75	

Centrifugal Pump				
Equipment	P-201	P-202	P-203	P-204
Volumetric flow (m3/s)	1.13×10^{-2}	2.08×10^{-2}	2.50×10^{-2}	8.21×10^{-3}
Density (kg/m3)	997.76	1,298.73	1,234.61	1,171.33
Pumping Head (m)	1.51	0.81	0.89	1.19
Utility Type	Electricity			
Utility per batch (MWh)	3.33×10^{-4}	1.06×10^{-3}	1.21×10^{-3}	2.83×10^{-4}
Cost per year (USD)	73.42	233.80	266.72	62.31

Separators					
Equipment	S-101	S-102	S-103	S-104	EL-101
Type	Sieve				Electrostatic Separator
Sieve Surface Area (m^2)	6.18	6.18	6.18	3.34	-
Utility Type	Electricity				
Utility per batch (MWh)	3.7×10^{-2}	3.7×10^{-2}	3.7×10^{-2}	3.7×10^{-2}	3.1×10^{-2}
Cost per year (USD k)	8.14	8.14	8.14	3.87	6.81

Heat Exchanger		
Equipment	E-201	E-202
Function	Cooler	Cooler
Type	CW	CW
mass required per batch (kg)	116,700.26	116,700.26
Cost per year (USD k)	182.54	182.54

Centrifuges						
Equipment	CE-101	CE-102	CE-103	CE-201	CE-202	CE-203
Type	Vertical Auto-Batch	Horizontal Auto-Batch		Horizontal Auto-Batch		
Utility Type	Electricity			Electricity		
Utility per batch (MWh)	7.4×10^{-2}	3.8×10^{-2}	4.0×10^{-2}	0.20	0.20	0.20
Cost per year (USD k)	16.33	8.43	8.86	44.06	44.06	44.06

Grinders		
Equipment	CR-101	SH-101
Type	Hammer Mill	Shredder
Utility Type	Electricity	
Utility per batch (MWh)	6×10^{-3}	5.3×10^{-2}
Cost per year (USD k)	1.36	11.67

Storage Tanks																	
Equipment	TK-101	TK-102	TK-103	TK-104	TK-105	TK-106	TK-107	TK-108	TK-109	TK-110	TK-111	TK-112	TK-201	TK-202	TK-203	TK-204	TK-205
Type	Cone Roof																
Orientation	Vertical																
Volume (m^3)	5.07	33.01	28.29	4.72	4.72	1.05	0.77	0.27	3.67	2.22	20	1.45	0.26	36.22	6.73	9.68	0.54
Material	Carbon Steel																

8.2. Economic Evaluation and Profitability Analysis

Economic evaluation and profitability analysis were done using total capital investment, production cost, Net Present Value (NPV), payback period and Internal rate of return (IRR) according to several financial assumptions. It was assumed that the plant is 100% debt – financed and would have a lifespan of 15 years based on industry standards including 3 years of start-up period [68]. Singapore's

corporate tax rate of 17% was applied and with depreciation throughout its lifespan of 15 years. Plant depreciation was assumed to be at 8% [35]. For the computation of payback period, the loan interest is 9% [69].

For NPV, straight line depreciation was assumed due to the ease of implementation and general usage across all industries to calculate the plant's Net Present Value (NPV) and its rate of return is assumed to be 15%. [35] Net Cash flow was determined by using net earnings after corporate tax thereafter deducting it by working capital (C_{WC}) and depreciable Capital (C_{TDC}).

IRR was not done as the NPV was in the negative range (See Table 15)

8.2.1. Total Capital Investment

CAPEX was repaid equally over the entire lifespan of the plant with no salvage value left was assumed at the end of the 15 years. Allocated cost for utilities and related facilities (C_{alloc}) was not included, as the plant would be purchasing the utilities from external parties. From Table 12, total bare module investment is the biggest contributor to the total capital investment with majority coming from hydrometallurgy process at 51.69%. Furthermore, working capital is derived based on 17.6% of the total permanent investment [35].

Table 12: Table of Total Capital Investment [35]

	Cost (mil USD)	**% Contribution to C_{TCI}**	**Equation Methodology**
Hydrometallurgy C_{BM}	63.27	51.69	Addition of all equipment cost
Mechanical C_{BM}	3.56	2.91	
Total Bare-Module Investment, C_{TBM}	66.83	54.59	Addition of Hydro C_{BM} & Mechanical C_{BM}
Cost of Site Preparation, C_{SITE}	10.02	8.19	Taken as 15% of C_{TBM}
Cost of service facilities, C_{SERV}	3.34	2.73	Taken as 5% of C_{TBM}
Allocated cost for off-site utility plants, C_{ALLOC}	0.00	-	-
Total Direct Permanent Investment, C_{TDC}	80.19	-	$C_{TBM} + C_{SITE} + C_{SERV} + C_{ALLOC}$
Cost of Contingencies and Contractor's Fee, C_{CONT}	14.44	11.79	Taken as 18% of C_{DPI}
Total Depreciable Capital, C_{TDC}	94.63	-	$C_{DPI} + C_{CONT}$
Cost of Land, C_{LAND}	1.89	1.55	Taken as 2% of C_{TDC}
Cost of Royalties, C_{ROYAL}	1.89	1.55	Taken as 2% of C_{TDC}
Cost of Plant Start-up, $C_{STARTUP}$	5.68	4.64	Taken as 10% of C_{TDC}
Total Permanent Investment, C_{TPI}	104.09	-	$C_{TDC} + C_{LAND} + C_{ROYAL} + C_{STARTUP}$
Working Capital, C_{WC}	18.32	14.97	Taken as 17.6% of C_{TPI}
Total Capital Investment, C_{TCI}	122.41	100.00	$C_{TPI} + C_{WC}$
Annualised Total Capital Investment, C_{TCI} (annualized)	15.19	-	Annualised by dividing C_{TPI} by 15 years of useful life

8.2.2. Total Production Cost

From Table 13, the biggest contributor to the total production cost is the total feedstock required for the process, 36.36% with mechanical feedstock playing a bigger part to it as the cost of the heavy liquid (SPT) is expensive and it required high amount also (refer to Table 8), even though it is a one-time purchase.

Table 13: Table of Total Production Cost [35, 70]

	Cost (mil USD)	**% Contribution to C**	**Methodology**
Hydrometallurgy Feedstock	13.29	14.64	-

Mechanical Feedstock	19.88	21.90	-
Feedstock, F	33.17	36.54	-
Hydro Utilities	0.19	0.21	-
Mech Utilities	7.52	8.28	-
Utilities, U	7.71	8.493	-
Labor-related costs, O	19.54	21.53	Wages assigned to be 16.5 USD/hour (based on Singapore's average wage rates). Therefore, O = 1.21*DW&B + TA + LAB
Maintenance, M	8.86	9.75	3.5%*CTDC + 1.3*4.5%*CTDC
Operating Overhead, OO	2.02	2.223	0.228*M
Property Taxes and Insurance, PTI	1.89	2.09	0.02* CTDC
Depreciation, D	7.58	8.356	8%*(CTDC-1.18Calloc)
Cost of Manufacturing, COM	80.77	-	COM = F + U + O+ M + OO + PTI +D
Selling Expense, SE	2.60	2.86	Taken as 3% of Sales Revenue
Direct Research, DR	4.16	4.58	Taken as 4.8% of Sales Revenue
Allocated Research, AR	0.43	0.48	Taken as 0.5% of Sales Revenue
Administrative expense, AE	1.73	1.91	Taken as 2% of Sales Revenue
Management Incentive Compensation, MIC	1.08	1.19	Taken as 1.25% of Sales Revenue
Total General Expenses, GE	10.01	-	GE=SE +DR+AR+AE+MIC
Total Production Cost, C	91.23	100.00	CTO=COM + GE

8.2.3. Revenue

Table 14: Table of Revenue

Product	**Lithium Carbonate**	**Mixed Hydroxides Precipitate (Cobalt, Nickel, Manganese)**	**Copper (Clean Aluminum/Copper AC Coils (free of steel))**	**Graphite**
Rate (USD$/metric ton)	37000 [71]	21600 [72]	3200 [65]	500 [73]
Mass (metric ton) Recovered/Year	1607.39	1126.17	700.31	1291.87
Total Revenue (USD$)/Year	$59,473,324.96	$24,325,229.49	$2,241,000.85	$645,933.01
Total Revenue (USD$)/Year	$86,685,488.31			

8.2.4. Plant Profitability Analysis

Table 15: Plant Profitability Overview

Total Production Cost (mil$/year)	90.78
Total Sales of products (mil$/year)	86.69
Gross Profit(mil$/year)	(4.09)
Depreciation (mil$/year)	7.57
Net Present Value, NPV (mil$)	- 98.44
Payback Period (years)	22.67
Return of Investment, ROI (%)	-2.77

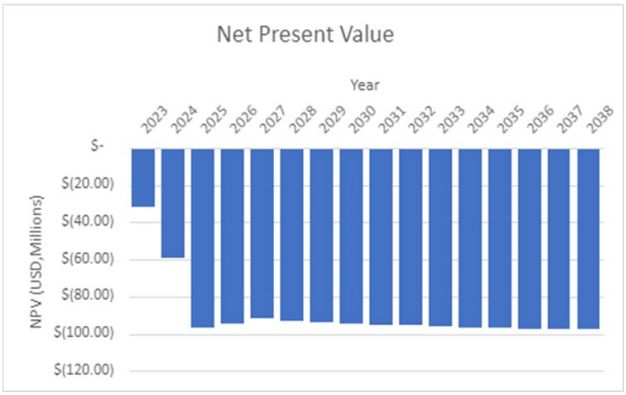

Figure 5: Graph of Net Present Value

Profitability of the plant determines the feasibility of plant construction, as it provides the plant's current value through NPV, the amount of investment returns from ROI and the payback period. From Table 15, it provides an overview of the plant profitability, it shows that the plant is making losses of 4.09 million annually and depreciation of 7.57 million annually which contributed to the negative NPV of 98.44 million. The whole project would need 22.67 years to pay back the original investment, which is not an attractive investment as the payback period is more than 4 years. ROI is also in the negative range; thus, all the financial indicators suggested that the plant is not profitable.

Since no reaction kinetics of the precipitation reaction were included in the simulation, the losses may be attributable to the inability to optimize it. In addition, calcium oxide was not recycled back, because 99.2% of it was disposed during the calciner process, that loses USD 298,022 (24508 tons) annually. Temperature was not considered during J-cost analysis because there was a lack of reaction kinetics information at various temperatures for this two-step leaching setup, thus the current setup might not be the most optimized.

For mechanical processes, ASPEN Plus was not able to simulate most of the operations (e.g. utilities, size and etc). Furthermore, certain conditions such as particle size, processing capacities etc were too specific, thus information was scarce. Equipment costing determined may not truly reflect the actual cost as some conditions were extrapolated and some were based on assumptions.

9. J-Cost/Profit Analysis and Dominant Design Variable (DDV) Ranking

This section explores various DDVs that can affect the costing of the LIB recycling plant. The main factors that affect the costing and processing capacity of the plant are batch reaction times and volume of materials in each unit operation. It is desired to keep the overall volume at a minimum so that smaller sized pressure vessels can be used. There will also be less energy required for heating and cooling processes downstream. The 4 main variables that affect these are: SA Pulp Density (SA PD), OA Pulp Density (OA PD), SA concentration and OA concentration. At the end of the analysis, the DDVs were ranked and the process was optimized based on the DDV ranking, thereafter the optimized process results were then compared with the base case results.

Only the hydrometallurgical section is used for DDV analysis. The mechanical process, albeit having a higher cost of raw materials, have a significantly lower utility and equipment cost compared to the hydrometallurgy process (Table 16). Additionally, the raw materials in the mechanical process cannot be changed as they include the LIBs to be recycled. As such, the focus for this section will be on the hydrometallurgy process.

Table 16:Table of Base Case Cost Breakdown

Raw material		**Energy**		**Equipment cost**	
Mech	**Hydro**	**Mech**	**Hydro**	**Mech**	**Hydro**
$21,720,878.79	$15,814,865.17	$189,510.38	$9,305,281.12	$3,559,650	$82,218,330.68

9.1. Hydrometallurgical Process

The primary contributors affecting the batch reaction times and volume of materials used are OA PD, SA PD, OA concentration and SA concentration. Other materials used in the recycling process include the LNMC metals which enter after being processed in the mechanical side, and K2CO3 and MgO which are used downstream to precipitate the metals. However, these reactants are used in a much lower volume compared to OA and SA as shown in Table 17. As such, the OA and SA streams were the best choices to be studied.

Table 17: Table of Volume of Raw Materials

Volume of materials (m^3)			
OA	SA	K2CO3	MgO
13.62	37.48	0.54	1.24

9.1.1. OA Pulp Density (OA PD)

OA PD was increased from 10% to 13%, with increments of 1%. As OA PD increases, the mass of OA and water entering in the feed stream decreases (Table 18, Section B). This is due to a lower volume of OA is needed to react with the mass of LIB scrap entering for first step leaching. Consequently, the raw material cost decreases and the overall volume handled by each unit operation decreases. As such smaller sized pressure vessels and heat exchanger with a lower surface area can be used (Table 18, Section D). Less reaction utility is needed to maintain reaction temperatures. The process heating and cooling utility is also lower (Table 18, Section C). The heat exchangers and agitators also require less utility at higher OA PD. OA PD has no effect on the batch reaction time for first step leaching. Overall, as OA PD increases from 10% to 13%, the costs for utility, raw material and equipment decreases (Table 18, Section A).

Table 18: Table of Summary of Changes when OA PD varies from 10% to 13%

		OA Pulp Density (%)	10	11	12	13
	A: J-Cost per year	J-Cost (USD)	$52,526,256.51	$52,079,742.19	$51,682,431.86	$51,347,487.67
	B: Raw Material Mass	Oxalic Acid (kg)	306.54	278.68	255.43	235.80
		Water (kg)	1.33×10^4	1.21×10^4	1.11×10^4	1.02×10^4
C: Utility per batch	Heating/ Cooling Streams	V-201 (kJ)	4.17×10^6	3.83×10^6	3.54×10^6	3.29×10^6
		R-201 (kJ)	1.04×10^7	9.59×10^6	8.89×10^6	8.30×10^6
	Heat Exchanger	E-201 / E-202 (kJ)	8.22×10^6	6.74×10^6	5.52×10^6	4.49×10^6
	Agitator	R-201 (kJ)	6.44×10^5	5.46×10^5	4.61×10^5	3.99×10^5
D: Equipment Sizing	Pressure Vessel	R-201 (m^3)	20.53	18.98	17.68	16.58
	Heat Exchanger Surface Area	E-201 (m^2)	84.74	69.40	56.79	46.27
	E: Reaction Duration	Batch Reaction Time for R-201 (h)	1.5			

9.1.2. SA Pulp Density (SA PD)

SA PD was increased from 6% (base case) to 9%, with increments of 1%. When PD increased, costs of raw material, utility and equipment decreased. The amount of SA and water added in as feed decreased as well. This meant less MgO was required to neutralize SA during NMC precipitation process (Table 19, Section B). This meant that the volume of the reactors required were lower as seen with reactors R-202 and R-203. Both reactors experienced a fall in reactor volume required when PD increased (Table 19, Section D). However, increasing the PD led to an increased reaction time. This could be attributed to the slower diffusion of reactants caused by a fall in the distance between the reactant particles. The increased reaction time causes an increase in the reactor utility required, shown in (Table 19, Section C). This increase in reactor utility required is countered by the fall in utility required for heating streams (less materials to heat) and utility required for agitation in the reactors (lower volume to agitate).

Table 19: Table of Summary of Changes when SA PD varies from 6% to 9%

		SA Pulp Density (%)	6	7	8	9
	A: J-Cost per year	J-Cost (USD)	$52,526,256.51	$47,819,785.67	$44,299,994.67	$41,926,964.67
	B: Raw Material Mass	Sulfuric Acid (kg)	1.10×10^4	9.45×10^3	8.27×10^3	7.35×10^3
		Water (kg)	4.87×10^4	4.36×10^4	3.98×10^4	3.69×10^4
		MGO (kg)	4.46×10^3	3.81×10^3	3.32×10^3	2.95×10^3
C: Utility per batch	Reaction	R-202 (kJ)	1.21×10^7	1.51×10^7	1.75×10^7	2.00×10^7
		R-203 (kJ)	4.09×10^7	3.42×10^7	2.92×10^7	2.55×10^7
	Heating/ Cooling Streams	R-202 (kJ)	1.37×10^7	1.18×10^7	1.04×10^7	9.30×10^6
		R-203 (kJ)	4.07×10^6	3.51×10^6	3.45×10^6	3.09×10^6
	Agitator	R-202 (kJ)	5.07×10^6	4.62×10^6	4.09×10^6	3.67×10^6
		R-203 (kJ)	4.11×10^6	3.15×10^6	2.31×10^6	1.76×10^6
D: Equipment Sizing	Pressure Vessel	R-202 volume (m^3)	52.32	45.54	40.47	36.49
		R-203 volume (m^3)	67.78	58.27	51.14	45.60
	E: Reaction Duration	Batch Reaction Time for R-202 (h)	2.00	2.50	2.90	3.30

9.1.3. OA Concentration

The OA concentration was increased from 0.25M to 1.0M, with increments of 0.25M. With increasing OA concentration, the amount of water and OA in the feed stream decreases and increases respectively (Table 20, Section B). As higher concentration OA is more expensive, the raw material cost increases from 0.25M OA to 1.0M OA. The volume of OA entering in the feed stream decreases with increasing OA concentration. This resulted in smaller pressure vessel sizes and heat exchanger surface area (Table 20, Section D), lower heating and cooling utility and lower utility for reactors, heat exchangers and agitators (Table 20, Section C). While the raw material cost increased with OA concentration, the overall cost still had a decreasing trend with increasing OA concentration (Table 20, Section A). The batch reaction time decreases with increasing OA concentration (Table 20, Section E) which would allow for a higher overall recycling rate for the plant.

Table 20: Table of Summary of Changes when OA Concentration varies from 0.25M to 1M

		OA Concentration (M)	0.25	0.50	0.75	1.00
	A: J-Cost per year	J-Cost (USD)	$52,526,256.51	$52,371,370.23	$52,336,097.50	$52,368,455.69
	B: Raw Material Mass	Oxalic Acid (kg)	3.07×10^2	6.13×10^2	9.20×10^2	1.23×10^3
C: Utility per batch	Reaction Utility	R-201 (kJ)	-4.00×10^7	-2.40×10^7	-1.70×10^7	-1.11×10^7
	Heating/ Cooling Streams	V-201 (kJ)	4.17×10^6	4.09×10^6	4.00×10^6	3.92×10^6
	Heat Exchanger	E-201/ E-202 (kJ)	8.22×10^6	7.82×10^6	7.46×10^6	7.13×10^6
	Agitator	R-201 (kJ)	6.44×10^5	4.12×10^5	3.16×10^5	2.27×10^5
D: Equipment Sizing	Pressure Vessel	R-201 (m^3)	20.53	20.16	19.79	19.40
	Heat Exchanger Surface Area	E-201 / E-202 (m^2)	84.74	80.58	76.77	73.45
	E: Reaction Duration	Batch Reaction Time for R-201 (h)	1.50	1.00	0.80	0.60

9.1.4. SA Concentration

The SA concentration was varied from 2.5M to 3.5M, with increments of 0.25M. When SA concentration increases, the utility costs tend to decrease. However, the raw material and equipment costs increases (Table 21, Section A). The fall in utility costs is caused by a combined effect of the reaction utility, stream heating utility and agitator utility (Table 21, Section C). For R-202, the magnitude of all three utilities fall with increasing SA concentrations. The increase in SA concentration caused a higher rate of reaction, by increasing the number of collisions between the reactants. This leads to a lower reaction and agitator utility as a shorter time is required for reaction completion. Conversely, for R-203, the magnitude of the three utilities increased with an increase in SA concentration. The increase in SA concentration meant that a higher amount of MgO was required to neutralize the additional SA during NMC precipitation process. This leads to a higher total volume in R-203, leading to higher utilities required for heating and agitation. (Table 21, Section D) also validates this by showing an increase in R-203 volume with a relatively constant R-202 volume. This then also justifies an increase in both the raw material and equipment costs with an increase in SA concentration.

Table 21: Table of Summary of Changes when SA Concentration varies from 2.5M to 3.5M

		SA Concentration (M)	2.50	2.75	3.00	3.25	3.50
	A: J-Cost per year	J-Cost (USD)	$49,690,259.59	$51,233,548.40	$52,526,255.93	$53,522,071.95	$54,543,914.54
	B: Raw Material Mass	Sulfuric Acid (kg)	9.19×10^{3}	1.01×10^{4}	1.10×10^{4}	1.19×10^{4}	1.29×10^{4}
		MGO (kg)	4.08×10^{3}	4.08×10^{3}	4.46×10^{3}	4.84×10^{3}	5.21×10^{3}
C: Utility per batch	Reaction Utility	R-202 (kJ)	1.82×10^{7}	1.52×10^{7}	1.21×10^{7}	1.03×10^{7}	9.05×10^{6}
		R-203 (kJ)	3.32×10^{7}	3.70×10^{7}	4.09×10^{7}	4.12×10^{7}	4.14×10^{7}
	Utility for Heating/ Cooling Streams	R-202 (kJ)	1.42×10^{7}	1.39×10^{7}	1.37×10^{7}	1.34×10^{7}	1.32×10^{7}
		R-203 (kJ)	4.13×10^{6}	4.15×10^{6}	4.07×10^{6}	4.01×10^{6}	3.93×10^{6}
	Agitator Utility	R-202 (kJ)	7.20×10^{6}	6.25×10^{6}	5.07×10^{6}	4.38×10^{6}	3.93×10^{6}
		R-203 (kJ)	3.48×10^{6}	3.85×10^{6}	4.11×10^{6}	4.19×10^{6}	4.04×10^{6}
D: Equipment Sizing	Pressure Vessel	R-203 volume (m^3)	64.28	66.32	67.78	67.96	68.14
	E: Reaction Duration	Batch Reaction Time for R-202 (h)	3	2.5	2	1.7	1.5

9.2. Variable Ranking to Determine Dominant Design Variable (DDV)

As the % change in the variables were significantly different between each of the variables mentioned above, to do a fair comparison of the % change in J-Cost, the % change in the variables had to be normalised into equivalent units of change as shown in Table 22.

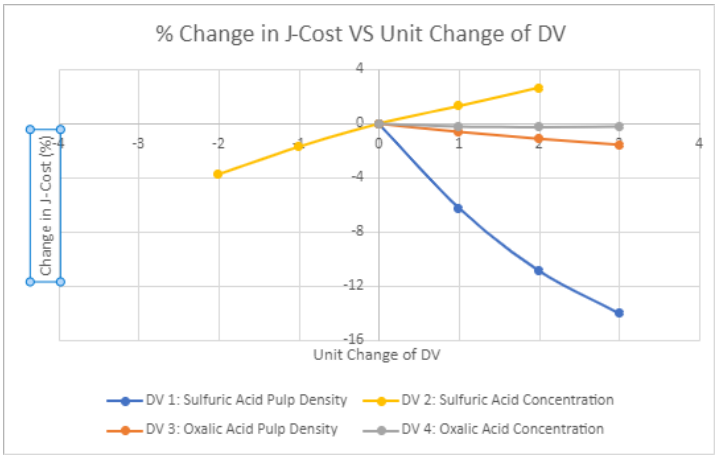

Figure 6: Figure of % Change in J-Cost VS Unit Change of DDV

Table 22: Table of Normalisation of DV variations into equivalent units of change of DV

	Sulfuric Acid		Oxalic Acid	
Unit Change of DV	Pulp Density (%)	Concentration (M)	Pulp Density (%)	Concentration (M)
-3	-	-	-	-
-2	-	2.5	-	-
-1	-	2.75	-	-
0	6	3	10	0.25
1	7	3.25	11	0.5
2	8	3.5	12	0.75
3	9	-	13	1

Table 23: Table of Ranking of DVs

Design Variable (DV)	Average % Change in Cost per Unit Change in DV (%)	Ranking
SA Pulp Density	4.67	1
SA Concentration	1.60	2
OA Pulp Density	0.52	3
OA Concentration	0.07	4

In order to understand how Figure 6 is used to rank the DDVs, the trends corresponding to each of the variables were compared. The larger the % change in J-Cost per unit change of the variable, the higher the effect the variable has on the equipment, utility and raw material cost. A common base case scenario was used for each of the DDVs. Based on the trends, it can be determined that the variable that gives the largest % change in J-Cost is the SA PD. A ranking of the variables and their effect on the % change in J-Cost was as shown in Table 23. As such it can be determined that SA PD is the first DDV and can be used for the cost optimisation of the base case.

9.3. Optimised Case and comparison with Base Case & DDV Case

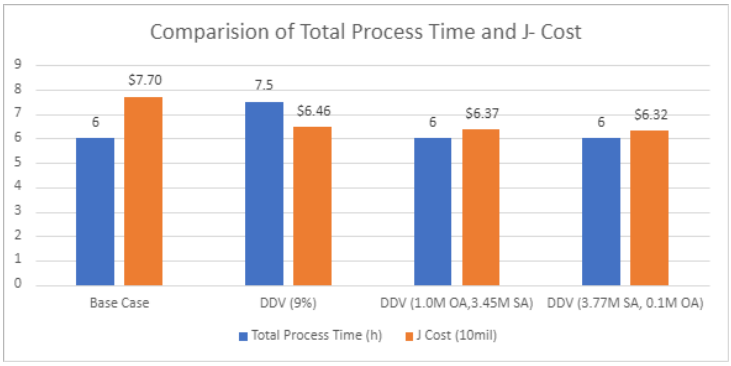

Figure 7: Chart of Comparison of Total Process Time and J-Cost

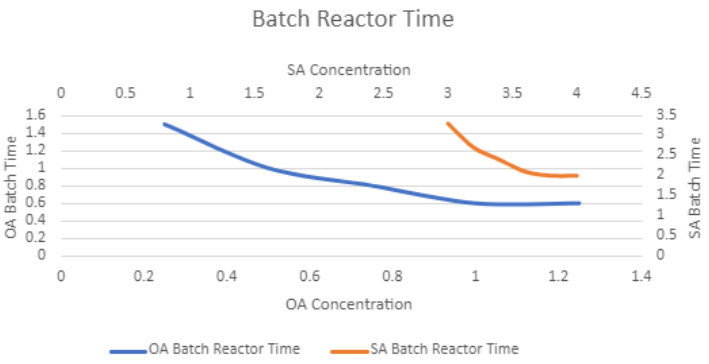

Figure 8: Graph of Batch Reactor Time VS Acid Concentration

The DDV SA PD 9% was chosen since it had highest percentage change in cost per unit change in DV. However, the process time for each batch increased to 7.5h (while the base case time is 6h). This decreases the recycling rate and decreases the amount of LIB that can be recycled each year. As such, to use a SA PD of 9%, further optimization was required to bring down the batch process time. The second DDV, SA concentration was then optimized. The process reaction time decreases with increasing SA concentrations as shown in Figure 8. Beyond a SA concentration of 3.77M, there was no further reduction in reaction time. Thus, the optimized case now included both SA PD 9% and SA concentration of 3.77M.

To meet the desired LIB recycling rate, the reaction time still had to decrease by 0.2h. The third DDV is OA PD. However, varying OA PD does not result in any batch process time changes. Thus, the fourth DDV, OA concentration, was used for further optimization instead. When OA concentration was varied with a SA PD of 9%, SA concentration of 3.77M and OA PD of 6%, 0.3M OA gave the optimal reaction time which would allow the plant to operate at the lowest cost while meeting the desired LIB recycling rate of 5000 metric tonnes per year that is shown in Figure 7.

10. Heat Integration and Exchanger Network

The two heat exchangers used in our design are both coolers for the reactors' exiting streams, hence we will not be able to do any form of inter-stream heat transfer. Furthermore, as a batch process, a heat exchanger network will not be viable due to the different durations that each reactor operates at, causing the streams to flow at different intervals. Therefore, there is no need for any heat integration and exchanger networks in this process design.

11. Waste Management

Take reference from the "PFD and Stream Summary.pdf" file for the breakdown of the waste streams.

11.1 Stream 5

H_2, despite not being a pollutant or greenhouse gas, can indirectly influence the concentration of other greenhouse gases in the atmosphere via its reaction with OH^-, which increases the levels of potent greenhouse gases such as methane and ozone [74]. As a result, although H_2 does not directly contribute to climate change, its emissions can have notable consequences on the Earth's climate system. The stream (containing trace N_2 as well) can be combusted with oxygen to form steam and trace amount of NOx [75]. The generated heat can be utilized to heat up the mixture in the calciner or other subsequent streams, resulting in reduced energy consumption. The resultant products will enter a blower to mix the gas with air to ensure that the emission of combustion products falls within the prescribed emission limits of 400mg/Nm^3 for NOx [76].

11.2 Stream 21

Considering the significant presence of CaO in the stream, recycling it would be a preferable option over disposal. With the addition of HCl to the stream, CaO will react with HCl to produce $CaCl_2$ [77], and the reaction of $CaCl_2$ with NaOH will yield $Ca(OH)_2$ [78].

The addition of the reagents mentioned above will also cause the reaction with other products in the stream and it will yield the following products eventually: $Ca(OH)_2$ (s), C (s), PVDF, NaCl (aq), NaF (aq), H_2O (l), and CO_2 (g) [78-82].

This product can be separated by physical states. The gas stream will be separated naturally, and the CO_2 can be released into the atmosphere (subjected to carbon tax) [83] One alternative solution to address the urgent issue of climate change is carbon capture and storage, even though it may be a costly approach [84]. For the solid and liquid waste, they can be separated using techniques such as filtration [85]. The separated solids can be further separated using a sieve since there is a size difference between C and PVDF (2cm) and $Ca(OH)_2$ (0.5-2.5μm) [86]. $Ca(OH)_2$ can be decomposed to yield CaO for recycling [87]. For the disposal of solids, since both PVDF and C are not considered hazardous [88, 89], it is possible to mix it with soil and dispose of it in a landfill. Liquid waste containing NaF and NaCl can be diluted with water, such that the concentration of F^- ions and Cl^- ions are below the permissible limits of 15mg/L and 1000mg/L, respectively [90], before releasing them. An alternative option is to dispose of both the solid and liquid waste at a licensed waste treatment facility.

11.3 Stream 29

As shown in Appendix D, the electrostatic separator's separation efficiency resulted in only 61.8% purity for the aluminium stream. This level of purity is insufficient to be sold [65] and would require the batch of aluminium to be discarded if no further action is taken. To address this issue, multiple passes through the electrostatic separator will be performed to increase the volume of copper recovered and improve the purity of the aluminium, ultimately allowing it to be sold.

11.4 Stream 56

A common way to neutralize acidic waste is by using lime ($Ca(OH)_2$) [91]. The addition of calcium hydroxide (lime) will result in the precipitation of CaC_2O_4, $Mg(OH)_2$, $CaSO_4$, $Ni(OH)_2$ and $Mn(OH)_2$ [92-96], leaving behind trace amounts of CaSO4 dissolved in water [97]. The solids and liquids can be separated by methods such as filtration [85]. Since $Mg(OH)_2$, CaC_2O_4 and $CaSO_4$ are considered non-toxic [98-100], while $Mn(OH)_2$ is considered safe below the concentration of $5mg/m^3$ [101] and $Ni(OH)_2$ is considered safe below the concentration of $1mg/m^3$ [102], the solids can be mixed with soil and — after ensuring the concentration of $Mn(OH)_2$ and $Ni(OH)_2$ is below $5mg/m^3$ and $1mg/m^3$ — disposed in a landfill. An alternative option is to dispose of it at a licensed waste treatment facility.

As for the liquid stream, it contained only a slight amount of dissolved $CaSO_4$, and since $CaSO_4$ is considered non-toxic [97], the stream can be diluted with more water, such that the concentration of dissolved solids is below the permissible limits of 3000mg/L [90] before being disposed.

11.5 Stream 62

This gaseous stream contained mostly water vapour and trace amount of OA. As water and OA are reagents for the reaction in R-201, this stream can be condensed and recycled back to the OA stream entering R-201, while ensuring the concentration of OA is 0.25M.

11.6 Stream 68

This stream contained mainly OA and potassium oxalate, and water. By neutralizing this stream with lime, calcium oxalate solids and potassium hydroxide will be formed [92, 103]. Since the separation of the solids (calcium oxalate) and the liquids (potassium hydroxide and water) can be done via methods such as filtration[85], the two by-products can be treated separately.

For calcium oxalate, since it is considered as non-toxic [99], it can be mixed with soil and sent to a landfill.

For the potassium hydroxide solution, it can be neutralized with hydrochloric acid to form KCl and water [104]. Since KCl is not considered hazardous [105], the resultant solution can be diluted with water, such that the concentration of Cl^- ions are below the permissible limits of 1000mg/L [90] before releasing them. An alternative option is to dispose of it at a licensed waste treatment facility.

12. Hazard and Operability Study (HAZOP)

HAZOP analysis was performed for reactor R-203. The surrounding area (node) of R-203 was isolated as seen in P&ID in Figure 9 and studied. Hazards due to deviations were identified with parameters such as flow, level, temperature, and corrosion, and with guide words such as no, less, more and reverse. Causes and consequences associated with the deviations were identified and the risk classification was done following the risk matrix in Appendix E. Initial HAZOP evaluation was performed with no existing safeguards, and recommendations were given after risk classification. Risk classification was done again with the recommended safeguards in place as shown in the HAZOP [Table 24].

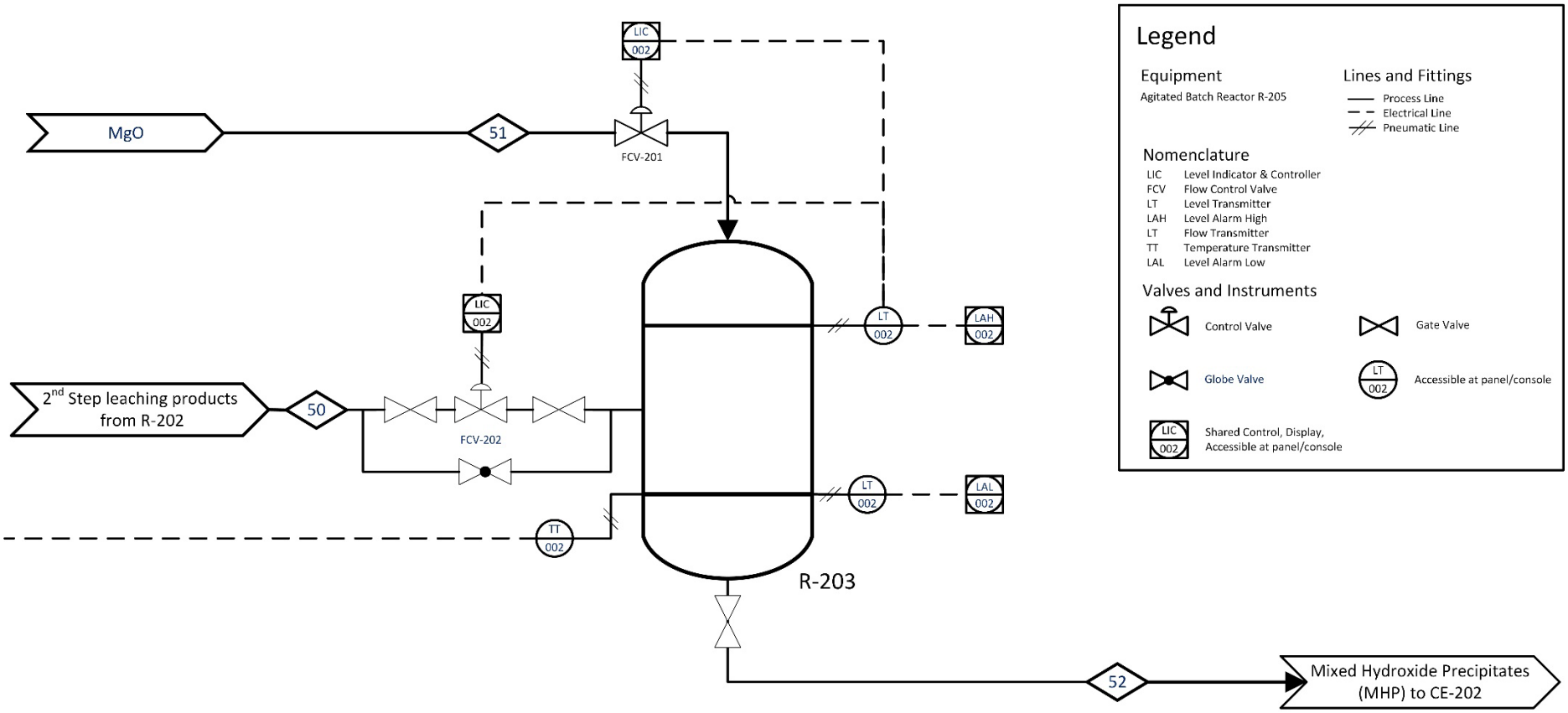

Figure 9: P&ID of R-203 with HAZOP

Table 24: HAZOP Analysis for Reactor R-203

Date		14-Apr-23													
Project		Recycling of Lithium-Ion Battery													
Node Description		Reactor R-205 is a jacketed batch reactor where feed stream containing NMC Sulfates flow in at 50°C and 1 atm. MgO, another reactant, is introduced to the reactor at 25°C and 1 atm. Reactor is operating at 50°C and 1 atm.													
Drawing		P&ID of R-205													
HAZOP Facilitator		Cassandre Chan Xiao Ying													
HAZOP Team		Indhu Jayabaskaran, Lim Junwei Darien, Teo Jun Wei, Ang Cheng Ting, Ashley Soh Wem Qi, Er Wei Leong Leonard, Yap Yan Lin													
No.	**Guide Word**	**Causes/Concerns**	**Consequences**	**Risk Classification Before Safeguards**			**Action No.**	**Recommendations**	**Risk Classification After Safeguards**			**Action by**	**Remarks**		
				Probability	**Consequence**	**Risk**			**Probability**	**Consequence**	**Risk**				
1.1	No Flow	Inlet line containing NMC sulfate blocked.	Product yield affected as no NMC Sulfates reacted and no NMC Hydroxides produced in R-205. No hazardous consequences identified.	3	0	0	-	Recommend monthly checks and maintance of pipelines to ensure no blockage.	1	0	0	-	-		
1.2		Inlet line containing MgO blocked.	Product yield affected as no MgO reacted and no NMC Hydroxides produced in R-205. No hazardous consequences identified.	3	0	0	-	Recommend monthly checks and maintance of pipelines to ensure no blockage.	1	0	0	-	-		
2.1	Low/ Less Flow	*See above on No Flow causes (pipe lines partially blocked instead of fully blocked)*	Slow production leading to operational delay. No hazardous consequences identified.	3	0	0	-	Recommend monthly checks and maintance of pipelines to ensure no blockage.	1	0	0	-	-		
3.1	High Flow	No credible causes identified	-	-	-	-	-	-	-	-	-	-	-		
4.1	Reverse Flow	No credible causes identified	-	-	-	-	-	-	-	-	-	-	-		
5.1	High Level/ Overflow	Blockage at outlet line, product stream unable to exit reactor.	Possible release of hazardous material from reactor due to high volume. Results in chemical burns to nearby operators.	3	3	9	-	a. Recommend monthly checks and maintance of pipelines to ensure no blockage. b. Add a level transmitter to the reactor to monitor its capacity. Attach a High Level indicator to the level transmitter so an alert will be sent out when reactor reaches 70% capacity. c. Attach a level indicator & controller to the control valve on inlet streams 40 & 41 to close off the flow via the flow control valves should reactor capacity hit 70%.	1	3	3	Process Engineer	Process Engineer to act based on the recommendation.		
6.1	Low Level/ Empty	*See above on No Flow and Less Flow Causes*	Slow production leading to operational delay. No hazardous consequences identified.	3	0	0	-	a. Recommend monthly checks and maintance of pipelines to ensure no blockage. b. Add level indicator so that volume of material in reactor can be monitored.	1	0	0	-	-		
7.1	High Temperature	Reactor jacket at higher temperature due to heat exchange errors.	Incorrect temperature for optimal reactions, resulting in lower yield and efficiency. Reactors are able to handle temperatures up to 400°C, which is not possible for heat exchanger to reach. No hazardous consequences identified.	2	0	0	-	Add temperature transmitter to the reactor. Regular monitoring of the temperature transmitter to ensure reactor is maintained at correct temperature.	1	0	0	-	-		
8.1	Low Temperature	Reactor Jacket at lower temperature due to heat exchange errors.	Incorrect temperature for optimal reactions, resuling in lower yield and efficiency. No hazardous consequences identified.	2	0	0	-	Add temperature transmitter to the reactor. Regular monitoring of the temperature transmitter to ensure reactor is maintained at correct temperature.	1	0	0	-	-		
9.1	Corrosion / erosion	Sulfuric acid reaction with the inner surface of reactor.	Leakage of hazardous material to surrounding. Results in chemical burns to nearby operators.	2	3	6	-	Recommend monthly checks and maintanace of reactor to check for corrosion.	1	3	3	Process Engineer	Process Engineer to act based on the recommendation.		

13. Bottlenecks and Recommendations

13.1: Recycling of CaO for pyrolysis reaction

As seen in Table 8, the amount of CaO being fed was 18724.50kg, and the amount of CaO exiting the calciner was 18567.84kg, which approximates to 99.2% of CaO. This suggests that CaO waste should be recycled instead of being disposed. The resources can be better used to cut down on raw material cost and reduce the wastage of precious materials. The waste stream can be treated as mentioned in section 11.2.

13.2: Improving the efficiency of Aluminium stream

According to Section 4, the copper stream's recovery rate was 68.6%, and the remaining copper was disposed of with the aluminium stream. As stated in Section 11.3, the purity of aluminium was 61.8%, rendering it unsellable. By implementing the waste treatment approach mentioned, both the purity and yield of copper and aluminium can be improved. Thus, the copper and aluminium can be sold to generate revenue.

13.3: More Experimental Data on 1st and 2nd Step Leaching Reactions

During the selection of design variables, reaction temperature was not chosen, as the data provided (Activation energy, Arrhenius constant) in the literature was based on one temperature for each leaching step reaction (Leaching Step 1: 80oC, Leaching Step 2: 60oC). This was because, by varying reaction temperature it could potentially affect a number of parameters such as the reaction duration, product recovery rates and, ultimately the utility and equipment cost.

13.4: Alternative Leaching Agent

Apart from sulfuric acid and oxalic acid, other acids or reagents could be studied as potential leaching agents that can result in higher recovery rates and faster reaction rates. As sulfuric acid is highly corrosive, this led to higher equipment requirements such as using more corrosion resistant material, thereby increasing the equipment cost. Therefore, less corrosive leaching agents could be chosen, which could potentially lead to cost savings.

14. Conclusion

All in all, LIBs have become increasingly important as a source of energy storage for electronic devices and electric vehicles. However, as the demand for LIBs grows, so does the need for safe and efficient recycling methods. The objective of designing a greener LIB recycling plant to extract lithium, cobalt, manganese and nickel had been achieved. Dismantled NMC 622 batteries underwent a pre-treatment process followed by a hydrometallurgy treatment process. The resulting product yield consists of 1607.39 tonnes of lithium carbonate, 1126.17 tonnes of mixed hydroxide precipitate, 700.31 tonnes of copper and 1291.87 tonnes of graphite, giving an annual revenue of $86 million. However, the economic aspect of our objective was not met. The process operated at an annual loss of $4.09 million, with a NPV of -$98.44 million. Considering this, it is not recommended to build this plant. Future studies could focus on optimising the choice of leaching agents that are more environmentally and economically friendly.

Appendix A: Processing Capacity Calculation

$Yearly\ input\ of\ batteries = 5000\ tonnes = 5000000kg$

$Cathode\ mass\ fraction = 0.252$ [106]

$Yearly\ cathode\ input = 0.252 \times 5000000 = 1258373.21kg$

$Daily\ cathode\ input = 1258373.21 \div 330 = 3813.25kg$

$Daily\ cathode\ input\ (accounting\ for\ 70\%\ of\ full\ capacity) = 3813.25 \div 0.7 = 5447.50kg$

$Cathode\ processing\ capacity\ per\ batch = 5447.50 \div 4 = 1361.88kg$

$Processing\ capacity\ per\ batch = 1361.88 \div 0252 = 5411.26\ kg$

Appendix B: Electric rotary calciner and rotary cooler

Estimation of Commercial Purchase Costs

We estimate the purchase cost of our designed H-101 and E-101 using Yong Ying's machinery product description and purchase price. Given the difference in length/diameter (L/D), using the calculated volumes of Yong Ying's machinery electric rotary calciner with the L/D kept constant at 16, "new" lengths and diameters is obtained for their corresponding purchased prices. D is used to correlate with the purchase price, assuming a direct relationship between D and cost. Similarly, the same approach is used for the E-101.

Using the method above, equation for electric rotary calciner is,

$Purchase\ Cost\ of\ = 122729 \times (Diameter) + 1.44$

$122729 \times (0.55) + 1.44\ = 67502.39\ USD$

Similarly, the equation for rotary cooler is,

$Purchase\ Cost\ = 24653 \times (Diameter) - 3832.80$

$24653 \times (0.55) - 3832.80\ = 9726.35\ USD$

Appendix C: Estimation of Heating and Cooling Duty

Table 25: Table of Rotary Calciner Heating and Cooling Duty [107-109]

Section A: Information

Parameters of Electric Rotary Calciner	
length (m)	8.80
Inner Diameter (m)	0.55
Inner radius, r_1 (m)	0.28
L/D	16.00
Thickness (m)	0.02
Outer Diameter (m)	0.57
Outer radius, r_2 (m)	0.01
Cross-sectional area (m^2)	0.24
Solid filling %	15.00
Cross-sectional area of solid (m2)	0.04
Volume of solid (m^3)	0.31
Residence time of solids (h)	0.17
Flow rate of solid (m^3/h)	1.88
Mass Flow rate of solid (kg/h)	6273.55

Temperatures in Electric Rotary Calciner	
Final Temperature of Solid, T_{out} (K)	573.15
Inlet Temperature of Solid, T_{in} (K)	298.15
Temperature of Wall, T_w (K)	605.15

Temperatures in Rotary Cooler	
Inlet Temperature of Water, $T_{water\ in}$ (K)	305.15
Outlet Temperature of Water, $T_{water\ out}$ (K)	322.15
Inlet Temperature of Solid, $T_{s\ in}$ (K)	573.15
Outlet Temperature of Solid, $T_{s\ out}$(K)	315.15

Section B: Calculating Areas

$Area\ of\ solids = 15\% \times (\pi {r_1}^2)$

$Area\ of\ solids = \frac{1}{2} {r_1}^2(\theta - \sin\theta)$

$\frac{1}{2} {r_1}^2(\theta - \sin\theta) = 0.0356m^2$

$\theta\ is\ found\ using\ solver, \theta = 1.89$

$A_{s1} = r_1\theta L = 4.58m^2$

$A_{g1} = (\pi D_1 - r_1\theta) \times L = 10.63m^2$

$A_{s2} = r_2\theta L = 4.74m^2$

$A_{g2} = (\pi D_2 - r_2\theta) \times L = 11.01m^2$

Section C: Inclination degree and rotational speed

$MRT = \frac{0.1026L^3}{\dot{V}} \times \left(\frac{\theta}{\beta}\right)^{1.054} \times \left(\frac{\dot{V}}{L^3 n}\right)^{0.981} \times \left(\frac{L}{D}\right)^{1.1}$

Chatterjee et al. (1983b)

$10 = \frac{0.1026 \times (8.8)^3}{0.03} \times \left(\frac{0.946}{\beta}\right)^{1.054} \times \left(\frac{0.03}{8.8^3 n}\right)^{0.981} \times \left(\frac{8.8}{0.55}\right)^{1.1}$

Using solver to find β and n

$\beta = 0.08$ and $n = 3.24\ rpm$

Section D: Calculating Overall Heat Gained by Solids and Gases

$Overall\ heat\ gained\ by\ solids\ and\ gas = \frac{LMTD}{(R_{total})} = 121.62 \times 579.43 = 70471.74\ W$

$\frac{1}{R_{total}} = \frac{1}{R_s} + \frac{1}{R_g} = 579.4345215 \frac{W}{K}$

$R_s = \frac{1}{h_s A_{s1}} + \frac{\delta}{\lambda A_{s2}} = \frac{1}{141.14 \times 4.58} + \frac{0.020}{15 \times 4.74} = 0.001828922 \frac{K}{W}$

$R_g = \frac{1}{h_g A_{g1}} + \frac{\delta}{\lambda A_{g2}} = \frac{1}{3.086 \times 10.63} + \frac{0.020}{15 \times 11.01} = 0.030614504 \frac{K}{W}$

$h_s = \left(\frac{\chi d_s}{k_g} + \frac{0.5}{\sqrt{2 k_s \rho_s c_{ps} \frac{n}{\beta}}}\right)^{-1}$ Li et al. (2005)

$h_s = \left(\frac{0.1 \times 3.07 \times 10^{-3}}{0.0444} + \frac{0.5}{\sqrt{2 \times 0.48 \times 3487.84 \times 761.83 \times \frac{3.24}{0.95}}}\right)^{-1} = 141.14 \frac{W}{m^2}.K$

$h_g = \frac{k_g}{D}\left[0.60 + \frac{0.387 Ra_D^{\frac{1}{6}}}{\left\{1 + \left(\frac{0.559}{Pr_g}\right)^{\frac{9}{16}}\right\}^{\frac{8}{27}}}\right]$ Churchill and chu [

$h_g = \frac{0.0444}{0.55}\left[0.60 + \frac{0.387 \times 27855801.27^{1/6}}{\left\{1 + \left(\frac{0.559}{0.691}\right)^{9/16}\right\}^{8/27}}\right] = 3.086 \frac{W}{m^2}.K$

$Ra_D = \frac{g \beta_v (T_w - T_g) D^3}{v_g \alpha_g} = \frac{9.81 \times 0.00174 \times (605.15 - 573.15) \times (0.55)^3}{0.0000475 \times 0.0000688} = 27855801.27$

$\Pr_g = \frac{\mu C_p}{k_g} = \frac{2.93 \times 10^{-5} \times 1046}{0.0444} = 0.691$

$LMTD = \frac{[(T]_w - T_{out}) - [(T]_w - T_{in})}{\ln\left(\frac{(T]_w - T_{out})}{(T]_w - T_{in})}\right)} = 121.62\ K$

R is thermal resistance $\left(K/W\right)$

h is heat transfer coefficient $\left(W/m^2 \cdot K\right)$

g is the acceleration due to gravity $\left(m^2/s\right)$

β_v volumetric expansion coefficient of gas (K^{-1})

T_w is temperature of wall (K)

T_g temperature of gas (K)

v_g is the kinematic viscosity of gas $\left(m^2/s\right)$

α_g is the thermal diffusivity of gas $\left(m^2/s\right)$

μ is dynamic viscosity $\left(kg/m \cdot s\right)$

C_p is specific heat $\left(J/kg \cdot K\right)$

k_g thermal conductivity of gas $\left(W/m \cdot K\right)$

Section E: Calculation of cooling required

$LMTD = \frac{[(T]_{s\ in} - T_{water\ out}) - [(T]_{s\ out} - T_{water\ in})}{\ln\left(\frac{[(T]_{s\ in} - T_{water\ out})}{[(T]_{s\ out} - T_{water\ in})}\right)} = 74.78\ K$

$Overall\ cooling = \frac{LMTD}{(R_{total})} = 74.78 \times 579.43 = 43333.82\ W$

Appendix D: Calculation of Purity of Aluminum Stream

Based on the operation of the electrostatic separator, the recovery of copper is 68.6% and the purity of the stream is 98.9%. With this information, the purity of aluminium stream can be calculated.

$Mass\ of\ copper = 693.88kg$
$Mass\ of\ copper\ in\ copper\ stream = 693.88 \times 0.686 = 476.00\ kg$
$Mass\ of\ copper\ stream = 476.00 \div 0.989 = 481.30kg$
$Mass\ of\ aluminium\ in\ copper\ stream = 481.30 - 476.00 = 5.29kg$

$Mass\ of\ aluminium = 357.30kg$
$Mass\ of\ aluminium\ in\ aluminium\ stream = 357.30 - 5.30 = 352.00kg$
$Mass\ of\ copper\ in\ aluminium\ stream = 693.88 - 476.00 = 217.88kg$
$Recovery\ of\ aluminium = 352.00 \div 357.30 = 98.5\%$
$Purity\ of\ aluminium\ stream = 352.00 \div (357.30 + 217.88) = 61.8\%$

Appendix E: HAZOP Risk Assessment Matrix

			Hazard Severity				
			1	2	3	4	5
			Very Low Negligible injury, no absence from work	Low Minor injury requiring first aid treatment	Medium Injury leading to a lost time accident	High Involving a single death or serious injury	Very High Multiple deaths
LIKELIHOOD	1	Very Unlikely A freak combination of factors would be required for an incident to result	1	2	3	4	5
	2	Unlikely A rare combination of factors would be required for an incident to result	2	4	6	8	10
	3	Possible Could happen when additional factors are present but otherwise unlikely to occur	3	6	9	12	15
	4	Likely Not certain to happen but an additional factor may result in an accident	4	8	12	16	20
	5	Very Likely Almost inevitable that an incident would result	5	10	15	20	25

Figure 10: HAZOP Risk Assessment Matrix

References

[1] A. Gawel, Cooper, Nathan, "What did COP27 accomplish and what actions can we expect as a result?," 11 2022.
[2] R. H. S. A. S. Cabinet Office, "UK and partners launch new measures at COP27 Solutions Day to drive progress on transition to Zero Emission Vehicles," 11 2022.
[3] "Behaviour of Lithium-Ion Batteries in Electric Vehicles," 2018.
[4] Z. J. B. Baum, Robert E., Yu, Xiang, Ma, Jia, "Lithium-Ion Battery Recycling─Overview of Techniques and Trends," vol. 7, pp. 712-719, 2 2022.
[5] B. Nikhil, Amber, Cai, Kota, Yuzawa, Joy, Zhang, Vinit, Joshi Fei, Fang, Giuni, Lee, Ryo, Harada, Shawn, Shin, "Batteries: The Greenflation Challenge," 3 2022.
[6] C. P. Yingchi Yang, "MHP emerges as preferred route to sulfate for international nickel market," 2022.
[7] J. Miller, "Cobalt Blue producing Mixed Hydroxide Product from new Broken Hill Pilot Plant," 2021.
[8] V. Velázquez-Martínez, Santasalo-Aarnio, Reuter, Serna-Guerrero, "A Critical Review of Lithium-Ion Battery Recycling Processes from a Circular Economy Perspective," vol. 5, p. 68, 11 2019.
[9] P. Xu, Tan, Darren HS, Gao, Hongpeng, Rose, Satchit, Chen, Zheng, "Recycling of Li-Ion Batteries for Electric Vehicles," 2022.
[10] H. Bae, Kim, Youngsik, "Technologies of lithium recycling from waste lithium ion batteries: a review," vol. 2, pp. 3234-3250, 2021.
[11] A. Siekierka, Bryjak, Marek, Razmjou, Amir, Kujawski, Wojciech, Nikoloski, Aleksandar N, Dumée, Ludovic F, "Electro-driven materials and processes for lithium recovery—A review," *Membranes,* vol. 12, no. 3, p. 343, 2022.
[12] M. Zhou, Li, Bang, Li, Jia, Xu, Zhenming, "Pyrometallurgical Technology in the Recycling of a Spent Lithium Ion Battery: Evolution and the Challenge," vol. 1, pp. 1369-1382, 10 2021.
[13] L.-F. Zhou, Yang, Dongrun, Du, Tao, Gong, He, Luo, Wen-Bin, "The Current Process for the Recycling of Spent Lithium Ion Batteries," vol. 8, 12 2020.
[14] P. Schiavi, Baldassari, Ludovica, Altimari, Pietro, Moscardini, Emanuela, Toro, Luigi, Pagnanelli, Francesca, "Process Simulation for Li-MnO2 Primary Battery Recycling: Cryo-Mechanical and Hydrometallurgical Treatments at Pilot Scale," vol. 13, p. 4546, 9 2020.
[15] M. Wang, Q. Tan, L. Liu, and J. Li, "A facile, environmentally friendly, and low-temperature approach for decomposition of polyvinylidene fluoride from the cathode electrode of spent lithium-ion batteries," *ACS Sustainable Chemistry & Engineering,* vol. 7, no. 15, pp. 12799-12806, 2019.
[16] X. Zhu, C. Zhang, P. Feng, X. Yang, and X. Yang, "A novel pulsated pneumatic separation with variable-diameter structure and its application in the recycling spent lithium-ion batteries," *Waste Management,* vol. 131, pp. 20-30, 2021.
[17] J. Diekmann *et al.*, "Ecological recycling of lithium-ion batteries from electric vehicles with focus on mechanical processes," *Journal of the electrochemical society,* vol. 164, no. 1, p. A6184, 2016.
[18] A. Salama, G. Richard, K. Medles, T. Zeghloul, and L. Dascalescu, "Distinct recovery of copper and aluminum from waste electric wires using a roll-type electrostatic separator," *Waste Management,* vol. 76, pp. 207-216, 2018.
[19] H. Al-Shammari and S. Farhad, "Heavy liquids for rapid separation of cathode and anode active materials from recycled lithium-ion batteries," *Resources, Conservation and Recycling,* vol. 174, p. 105749, 2021.
[20] K. S. Chabhadiya, Rajiv Ranjan and P. Pathak, "Two-step leaching process and kinetics for an eco-friendly recycling of critical metals from spent Li-ion batteries," vol. 9, p. 105232, 6 2021.

[21] A. Verma, A. J. Henne, D. R. Corbin, and M. B. Shiflett, "Lithium and Cobalt Recovery from LiCoO2 Using Oxalate Chemistry: Scale-Up and Techno-Economic Analysis," *Industrial & Engineering Chemistry Research,* vol. 61, no. 15, pp. 5285-5294, 2022.
[22] N. Safitri, Mubarok, M. Zaki, Winarko, Ronny, Tanlega, Zela, "Recovery of nickel and cobalt as MHP from limonitic ore leaching solution: Kinetics analysis and precipitate characterization," p. 020030, 2018.
[23] A. Haghtalab, Papangelakis, Vladimiros G, Zhu, Xuetang, "The electrolyte NRTL model and speciation approach as applied to multicomponent aqueous solutions of H2SO4, Fe2(SO4)3, MgSO4 and Al2(SO4)3 at 230–270°C," vol. 220, pp. 199-209, 6 2004.
[24] E. C. Carlson, "Don't Gamble With Physical Properties For Simulations," vol. 92, pp. 35-46, 10 1996.
[25] A. Tech, "Aspen physical property system 11.1," *Aspen Technology, Inc., Cambridge, MA, USA,* 2001.
[26] "Waste battery shredder machine."
[27] M. Sebastian Escotet-Espinoza, C. J. Foster, and M. Ierapetritou, "Discrete Element Modeling (DEM) for mixing of cohesive solids in rotating cylinders," *Powder Technology,* vol. 335, pp. 124-136, 2018/07/15/ 2018.
[28] D. W. Dahlstrom, "Rotary Tube Calciners," *Carbide, Nitride and Boride Materials Synthesis and Processing,* pp. 631-636, 1997.
[29] T. Kohav, J. T. Richardson, and D. Luss, "Axial dispersion of solid particles in a continuous rotary kiln," *AIChE Journal,* vol. 41, no. 11, pp. 2465-2475, 1995.
[30] S. Gudić, L. Vrsalović, A. Matošin, J. Krolo, E. E. Oguzie, and A. Nagode, "Corrosion Behavior of Stainless Steel in Seawater in the Presence of Sulfide," *Applied Sciences,* vol. 13, no. 7, p. 4366, 2023.
[31] R. Roger Francis, "The performance of stainless steels in concentrated sulphuric acid."
[32] R. GmbH, "Operating instructions for sieving machinetype AS300 control," 2012.
[33] R. GmbH, "Sieve Shaker AS 300 Test Report," 2006.
[34] *VANER plate electrostatic separator*. Available: https://www.alibaba.com/product-detail/VANER-plate-electrostatic-separator-electrostatic-separator_1600185474698.html?spm=a2700.galleryofferlist.0.0.5da04accPfbHCD
[35] W. D. Sieder, Seader, JD, Lewin, Daniel R, Widagdo, S, "Product and process design principles," ed: John Wiley & Sons: Hoboken, NJ, USA, 2004.
[36] "Fact Sheet Centrifuge Safery."
[37] A. N. Schofield, "Cambridge geotechnical centrifuge operations," *Geotechnique,* vol. 30, no. 3, pp. 227-268, 1980.
[38] A. Gomez-Martin *et al.*, "Opportunities and Challenges of Li2C4O4 as Pre-Lithiation Additive for the Positive Electrode in NMC622|| Silicon/Graphite Lithium Ion Cells," *Advanced Science,* vol. 9, no. 24, p. 2201742, 2022.
[39] J. S. Browning, *Heavy liquids and procedures for laboratory separation of minerals* (no. 8007). US Department of the Interior, Bureau of Mines, 1961.
[40] H. B. Møller, I. Lund, and S. G. Sommer, "Solid–liquid separation of livestock slurry: efficiency and cost," *Bioresource Technology,* vol. 74, no. 3, pp. 223-229, 2000/09/01/ 2000.
[41] GeoLiquids, "Sodium Polytungstate (SPT) Safety Data Sheet," 2017.
[42] "316L Stainless Steel Chemical Compatibility Chart," 2022.
[43] S. Hall, *Rules of thumb for chemical engineers*. Butterworth-Heinemann, 2017.
[44] A. S. Afolabi, J. H. Potgieter, A. S. Abdulkareem, and N. Fungura, "Effect of tempering temperature and time on the corrosion behaviour of 304 and 316 austenitic stainless steels in oxalic acid," *World Academy of Science, Engineering and Technology,* vol. 79, pp. 87-91, 2011.
[45] R. Brogan, "Shell and tube heat exchangers," in *Thermopedia*: Begel House Inc., 2011.
[46] D. W. Green and M. Z. Southard, *Perry's chemical engineers' handbook*. McGraw-Hill Education, 2019.
[47] R. Sinnott, "Coulson and Richardson's Chemical Engineering Volume 6 (Design)," ed: Pergamon Press, 1999.
[48] E. Toolbox, "Metals, Metallic Elements and Alloys - Thermal Conductivities," 2005.
[49] S. Wang, "Suspension of high concentration slurry in agitated vessels," RMIT University, 2010.
[50] I.-S. Forest, "The corrosion resistance of nickel-containing alloys in sulfuric acid and related compounds," *INCO The International Nickel Company,* 1983.
[51] N. Sonawane, "Two-Phase Separator Design Basics."
[52] W. Svrcek and W. Monnery, "Design two-phase separators within the right limits," *Chemical engineering progress,* vol. 89, no. 10, pp. 53-60, 1993.
[53] "Different Types of Pumps," 2022.
[54] PUB, "Water Price."
[55] EMA, "Electricity Prices."
[56] TLV, "Steam Unit Cost."
[57] IndiaMART, "Oxalic Acid, For Industrial."
[58] IndiaMART, "Gangotri Powder Calcium Oxide USP JP for Industrial."
[59] M. Farish, "EV battery recycling: cost and components," 16 November 2020.
[60] IndiaMART, "White Sulphuric Acid Powder."
[61] IndiaMART, "Powder Potassium Carbonate, For Industrial, Packaging Type: Bag."
[62] "Magnesium Oxide 90% powder bulk industrial grade price."
[63] IndiaMART, "Sodium Polytungstate."
[64] "Single Cylinder Rotary Cooling Machine/Rotary Cooler."
[65] R. R. Center. *Pricing*. Available: https://www.reliablerecyclingcenter.com/pricing/
[66] "China electric rotary kiln indirect external heating kiln / Activated Carbon Regeneration Furnace rotary kiln price for sale."
[67] "PP ABS PS waste battery and tyre shredder machine plastic recycle double shaft shredder machine."
[68] R. Hillebrand, "TECHNICAL WHITE PAPER LIFE CYCLE POLICY FOR THE CHEMICAL, PETROCHEMICAL AND PHARMACEUTICAL INDUSTRIES," 09 August 2007.
[69] Linkflow, "SME Business Loan Interest Rate in Singapore."
[70] E. R. Institute, "Machine Operator Salary In Singapore," 2023.
[71] Statista, "Average lithium carbonate price from 2010 to 2022," 2022.
[72] "LME Nickel."
[73] "Graphite Pricing," 2022.
[74] M. B. Bertagni, S. W. Pacala, F. Paulot, and A. Porporato, "Risk of the hydrogen economy for atmospheric methane," *Nature communications,* vol. 13, no. 1, p. 7706, 2022.
[75] M. C. Lee, S. B. Seo, J. Yoon, M. Kim, and Y. Yoon, "Experimental study on the effect of N2, CO2, and steam dilution on the combustion performance of H2 and CO synthetic gas in an industrial gas turbine," *Fuel,* vol. 102, pp. 431-438, 2012.

[76] "Environmental Protection and Management (Air Impurities) Regulations," *ENVIRONMENTAL PROTECTION AND MANAGEMENT ACT,* vol. CHAPTER 94A, SECTION 77, 2008.
[77] R. Bie, S. Li, and L. Yang, "Reaction mechanism of CaO with HCl in incineration of wastewater in fluidized bed," *Chemical engineering science,* vol. 60, no. 3, pp. 609-616, 2005.
[78] A. Mas Herrador, "Thermodynamic and experimental study of the fluoride recovery from Spent Pot Lining recycling process by precipitation of calcium fluoride," Universitat Politècnica de Catalunya, 2020.
[79] "CHEMICAL RESISTANCE GUIDE (PVDF)," 2014.
[80] C. Liu *et al.*, "The intensified leaching behavior of potassium from phosphorus-potassium associated ore in HCl-CaF2 system with surfactant: Part I kinetics and modelling," *Separation and Purification Technology,* vol. 212, pp. 89-100, 2019.
[81] W. Miglietti and F. Blum, "Advantages of fluoride ion cleaning at sub-atmospheric pressure," *Engineering Failure Analysis,* vol. 5, no. 2, pp. 149-169, 1998.
[82] P. Scandiffio, T. Mantilla, F. Amaral, F. França, R. Basting, and C. Turssi, "Anti-erosive effect of calcium carbonate suspensions," *Journal of Clinical and Experimental Dentistry,* vol. 10, no. 8, p. e776, 2018.
[83] "Carbon Tax," 2023.
[84] R. M. Cuéllar-Franca and A. Azapagic, "Carbon capture, storage and utilisation technologies: A critical analysis and comparison of their life cycle environmental impacts," *Journal of CO2 utilization,* vol. 9, pp. 82-102, 2015.
[85] R. G. Holdich, A. Rushton, and A. S. Ward, *Solid-liquid filtration and separation technology*. John Wiley & Sons, 2008.
[86] T. Komabayashi, R. N. D'souza, P. C. Dechow, K. E. Safavi, and L. S. Spångberg, "Particle size and shape of calcium hydroxide," *Journal of endodontics,* vol. 35, no. 2, pp. 284-287, 2009.
[87] A. Gupta, P. D. Armatis, P. Sabharwall, B. M. Fronk, and V. Utgikar, "Thermodynamics of Ca (OH) 2/CaO reversible reaction: Refinement of reaction equilibrium and implications for operation of chemical heat pump," *Chemical Engineering Science,* vol. 230, p. 116227, 2021.
[88] "Safety Data Sheet PVDF," 2013.
[89] "Safety Data Sheet Carbon," 2015.
[90] "REQUIREMENTS FOR DISCHARGE OF TRADE EFFLUENT INTO THE PUBLIC SEWERS."
[91] H. W. Gehm, "Neutralization of acid waste waters with an up-flow expanded limestone bed," *Sewage Works Journal,* pp. 104-120, 1944.
[92] D. Rao and J. Tewari, "Suppression of the symptoms of American leaf spot of coffee with calcium hydroxide," *Plant disease,* vol. 72, no. 8, pp. 688-690, 1988.
[93] S. Ziegenheim, M. Szabados, Z. Kónya, Á. Kukovecz, I. Pálinkó, and P. Sipos, "Differential precipitation of Mg (OH) 2 from CaSO4· 2H2O using citrate as inhibitor—A promising concept for reagent recovery from MgSO4 waste streams," *Molecules,* vol. 25, no. 21, p. 5012, 2020.
[94] R. Zahedi and S. J. Mirmohammadi, "Sulfate removal from chemical industries' wastewater using ettringite precipitation process with recovery of Al (OH) 3," *Applied Water Science,* vol. 12, no. 9, p. 226, 2022.
[95] N. Al-Mansi and N. A. Monem, "Recovery of nickel oxide from spent catalyst," *Waste management,* vol. 22, no. 1, pp. 85-90, 2002.
[96] A. Pohl, "Removal of heavy metal ions from water and wastewaters by sulfur-containing precipitation agents," *Water, Air, & Soil Pollution,* vol. 231, no. 10, p. 503, 2020.
[97] PubChem, "Calcium Sulfate Compound Summary."
[98] (2021). *SAFETY DATA SHEET Magnesium Hydroxide*. Available: https://www.fishersci.com/store/msds?partNumber=M342500&productDescription=MAGNESIUM+HYDROX+USP%2FFCC+500G&vendorId=VN00033897&countryCode=US&language=en
[99] W. Schadel and W. Walter, "Calcium Oxalate Crystals in the Roots of Sweet Potato1," *Journal of the American Society for Horticultural Science,* vol. 105, no. 6, pp. 851-854, 1980.
[100] (2015). *Safety Data Sheet Calcium Sulfate*. Available: https://beta-static.fishersci.com/content/dam/fishersci/en_US/documents/programs/education/regulatory-documents/sds/chemicals/chemicals-c/S25230.pdf
[101] "Manganese Hydroxide (Hazardous Agents)," 2023.
[102] "Nickel(II) hydroxide Hazardous Agent."
[103] H. Chen, P. Feng, S. Ye, and W. Sun, "The coupling effect of calcium concentration and pH on early hydration of cement," *Construction and Building Materials,* vol. 185, pp. 391-401, 2018.
[104] W. J. Biermann, "The relative enthalpies of concentrated potassium hydroxide solutions," *Canadian Journal of Chemistry,* vol. 38, no. 1, pp. 57-60, 1960.
[105] "Potassium Chloride Safety Data Sheet," 2022.
[106] A. D. Accardo, Giovanni Musa, Marco Luigi Spessa, Ezio, "Life Cycle Assessment of an NMC Battery for Application to Electric Light-Duty Commercial Vehicles and Comparison with a Sodium-Nickel-Chloride Battery," vol. 11, p. 1160, 1 2021.
[107] S.-Q. Li, L.-B. Ma, W. Wan, and Q. Yao, "A Mathematical Model of Heat Transfer in a Rotary Kiln Thermo-Reactor," *Chemical Engineering & Technology,* vol. 28, no. 12, pp. 1480-1489, 2005.
[108] D. R. Nhuchhen, P. Basu, and B. Acharya, "Investigation into overall heat transfer coefficient in indirectly heated rotary torrefier," *International Journal of Heat and Mass Transfer,* vol. 102, pp. 64-76, 2016/11/01/ 2016.
[109] X. Y. Liu and E. Specht, "Mean residence time and hold-up of solids in rotary kilns," *Chemical Engineering Science,* vol. 61, no. 15, pp. 5176-5181, 2006/08/01/ 2006.